

Molecular Physics

An International Journal at the Interface Between Chemistry and Physics


ISSN: (Print) (Online) Journal homepage: <https://www.tandfonline.com/loi/tmph20>


Testing the limitations of harmonic approximation in the determination of Raman intensities

Ankit Raj, Yen-Bang Chao & Henryk A. Witek


To cite this article: Ankit Raj, Yen-Bang Chao & Henryk A. Witek (2022) Testing the limitations of harmonic approximation in the determination of Raman intensities, Molecular Physics, 120:19-20, e2069613, DOI: [10.1080/00268976.2022.2069613](https://doi.org/10.1080/00268976.2022.2069613)


To link to this article: <https://doi.org/10.1080/00268976.2022.2069613>

 View supplementary material 

 Published online: 04 May 2022.


 Submit your article to this journal 

 Article views: 167

 View related articles 

 View Crossmark data 

Testing the limitations of harmonic approximation in the determination of Raman intensities

Ankit Raj , Yen-Bang Chao and Henryk A. Witek 

Department of Applied Chemistry and Institute of Molecular Science, National Yang Ming Chiao Tung University, Hsinchu, Taiwan

ABSTRACT

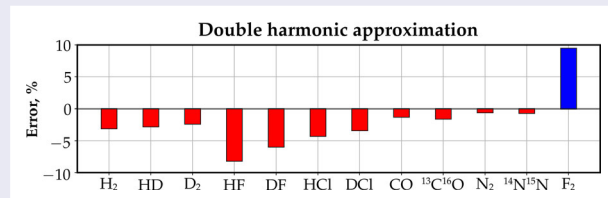
Raman intensities in molecular spectra are usually computed within double harmonic approximation. This procedure relies on treating a vibrating molecule as a collection of harmonic oscillators and on the assumption that polarisability tensor invariants display linear variations around the molecular equilibrium geometry. This methodology, originally formulated by Placzek, constitutes the theoretical foundation for computing Raman intensities in standard quantum chemistry packages. However, the two assumptions underlying double harmonic approximation have not been sufficiently tested. In this work, we employed exact anharmonic ro-vibrational wave functions and distance-dependent polarisability invariants together with their harmonic approximants to investigate the discrepancies in Raman intensities of the fundamental transitions in 12 diatomic molecules, caused by double harmonic approximation. We found that: (i) the errors in total Raman intensities were between -8.2% and $+9.5\%$, (ii) the largest discrepancy was observed for F_2 , where the polarisability invariants could not be adequately modelled by their linear approximants, and (iii) quantum chemical methods fail to predict reliable polarisability invariants at non-equilibrium molecular geometries; the associated errors in Raman intensities are huge and completely overshadow the shortcomings of double harmonic approximation. We communicate here an urgent need for developing accurate methods capable of computing reliable polarisabilities also at distorted geometries.

ARTICLE HISTORY

Received 29 January 2022
Accepted 8 April 2022

KEYWORDS

Polarisability; diatomic molecules; polarisability invariants; Raman intensities; Raman spectroscopy



1. Introduction

Raman spectroscopy is a well established branch of vibrational spectroscopy. Theoretical determination of Raman transition frequencies and the corresponding intensities comprises an important part of spectroscopic analysis. Theoretical foundations for this procedure were laid by Placzek [1] who used the polarisability tensor and vibrational wave functions as building blocks of his theory. In his work, the first-order induced dipole P_ρ along a Cartesian axes ρ , is expressed as a function of the polarisability

α and the incident electric field E_σ as

$$(P_\rho)_{v_f, v_i} = \langle \alpha_{\rho\sigma} \rangle_{v_f, v_i} E_\sigma \quad (1)$$

where $\langle \alpha_{\rho\sigma} \rangle_{v_f, v_i}$ represents the matrix element of polarisability connecting the initial state i to the final state f , which is determined as

$$\langle \alpha_{\rho\sigma} \rangle_{v_f, v_i} = \langle \psi_{v_f} | \alpha_{\rho\sigma}(\mathbf{Q}) | \psi_{v_i} \rangle \quad (2)$$

with $\alpha_{\rho\sigma}$ being the geometry-dependent molecular polarisability expressed as function of normal coordinates

\mathbf{Q} , $\alpha_{\rho\sigma} \equiv \alpha_{\rho\sigma}(\mathbf{Q})$. Polarizability is then expanded at the equilibrium molecular geometry as a Taylor series in \mathbf{Q} to obtain

$$\alpha_{\rho\sigma} = (\alpha_{\rho\sigma})_0 + \sum_k \left(\frac{\delta\alpha_{\rho\sigma}}{\delta Q_k} \right)_0 Q_k + \frac{1}{2} \sum_l \sum_k \left(\frac{\delta^2\alpha_{\rho\sigma}}{\delta Q_k \delta Q_l} \right)_0 Q_k Q_l + \dots \quad (3)$$

Substituting the above expansion for polarisability truncated at the first-order, and using harmonic oscillator wave functions for ψ in Equation (2) while working under the assumption of electrical harmonicity gives

$$\begin{aligned} \langle \alpha_{\rho\sigma} \rangle_{v_f, v_i} &= (\alpha_{\rho\sigma})_0 \left\langle \prod_k \phi_{v_f, k}(Q_k) \prod_k \phi_{v_i, k}(Q_k) \right\rangle \\ &+ \sum_{k'} \left(\frac{\delta\alpha_{\rho\sigma}}{\delta Q_{k'}} \right)_0 \\ &\times \left\langle \prod_k \phi_{v_f, k}(Q_k) | Q_{k'} | \prod_k \phi_{v_i, k}(Q_k) \right\rangle, \quad (4) \end{aligned}$$

which consists of two terms.¹ Using selection rules derived from harmonic-oscillator functions (see Section S1 in the supplementary material for more details), the zeroth-order term corresponds to Rayleigh scattering, while the latter term, containing the first-derivatives of polarisability corresponds to Raman scattering.

The above discussion based on the harmonic approximation constitutes the primary approach to the computation of Raman intensities [2].² Both formalisms for normal coordinate analysis and the resulting intensity analysis rest on the harmonic approximation. Consequently, almost all quantum chemistry programs available at present employ this double harmonic approximation for the computation of vibrational intensities, with truncation of polarisability invariants at the first order. While a great deal of work has been done regarding the discrepancy of harmonic transition frequencies with experimental results [3–11], a similar discussion pertinent to Raman intensities is limited [12,13]. The question to be answered is: What is the error associated with the assumption of the electrical harmonicity? In other words, how accurate are the Raman intensities computed under the harmonic approximation?

There are a few challenges to overcome in order to reliably answer these questions. The first one is to obtain accurate state specific wave functions for the studied molecules, and the second is to obtain reliable polarisabilities expressed as a function of the vibrational coordinates. These issues limit the choice of the possible molecules which can be studied in this context.

For diatomic molecules, the exact state-specific vibrational wave functions can be readily obtained beyond the harmonic approximation. In contrast, for larger molecules this is significantly harder. In computation of *ab-initio* polarisabilities, the accuracy of the results depends to a large extent on the choice of the quantum-chemical technique used for the calculations and on the choice of the basis sets used to construct the electronic wave function. Thus, it becomes computationally challenging to reliably perform tests on the harmonic approximation on larger molecular systems, where the quantum chemical calculations become expensive or even infeasible. Thus, smaller molecules are preferred for such a study. In the case of diatomic molecules, the polarisability can be naturally expressed as a function of the internuclear distance. In view of these considerations, we limit ourselves in the current study to a series of diatomic molecules containing from two to 18 electrons.

For diatomic molecules, several experimental and theoretical studies have been reported in the literature which indirectly expose the errors originating from the double harmonic approximation. Herman and Wallis discussed the centrifugal distortion arising from the vibration-rotation coupling during accurate determination of infrared intensities [14]. Similar study for the Raman intensities was performed by James and Klemperer [15]. In these works, the diatomic molecule under study was assumed to behave as a harmonic oscillator, and the centrifugal term $J(J+1)/2\mu r^2$ was approximated as a 2–3 term expansion over the reduced internuclear distance, ξ , defined as $\xi = (r - r_e)/r_e$. Polarizability anisotropy $\gamma = \alpha_{\parallel} - \alpha_{\perp}$, an invariant of the polarisability tensor α , governing the intensities of the O- and S-branches was approximated as a Taylor series expansion over ξ

$$\gamma(\xi) = \gamma_0 + \gamma_1 \xi + \frac{1}{2} \gamma_2 \xi^2 + \dots \quad (5)$$

where $\gamma_1 = \frac{\partial\gamma}{\partial r}$ and $\gamma_2 = \frac{\partial^2\gamma}{\partial r^2}$, while retaining up to three terms in the expansion. Using perturbation theory or numerical solutions, the correction factors (usually referred to as the Herman-Wallis factors) were approximated as functions of derivatives of polarisability anisotropy (γ_n), rotational constant (B_e), vibrational constant (ω_e) and the rotational quantum number (J). Alternatively, using known values of molecular constants and the determined Herman-Wallis factors, the values of derivatives of polarisability anisotropy for equilibrium internuclear distance were obtained by analysing intensities from acquired Raman spectra. The first derivative of polarisability anisotropy (γ_1) for H_2 and D_2 were determined by Asawaroengchai and Rosenblatt [16]. Hamaguchi and coworkers employed a simplified expansion

[17,18] given by

$$\frac{\gamma(\xi)}{\gamma_0} = 1 + \frac{\gamma_1}{\gamma_0} \xi + \frac{1}{2} \frac{\gamma_2}{\gamma_0} \xi^2 + \dots \quad (6)$$

and reported the numerical value of $(\gamma_1/\gamma_0)_{r_e}$ and $(\gamma_2/\gamma_0)_{r_e}$ for the same molecules. In this approach, the calculated Raman intensities were fitted using non-linear least squares regression to experimental intensities for O0- and S0-branch lines of H₂ and D₂, obtaining the values of $(\gamma_1/\gamma_0)_{r_e}$ and $(\gamma_2/\gamma_0)_{r_e}$ as fit parameters along with the intensity response curve of the spectrometer. Further, a similar analysis performed for N₂ revealed that the inclusion of the second derivatives in Equations (5) and (6) is less important than for H₂ [17–19]. In our earlier work, we have investigated the effects of centrifugal distortion to the Raman intensities of purely rotational transitions in H₂, HD and D₂, and examined the importance of including higher order derivatives of polarisability invariants in the process of determination of the Raman intensities [20]. This work revealed that Taylor series expansion up to the second order yields an excellent representation of both the invariants around r_e .

We start our analysis by performing accurate computations of Raman intensities determined from accurate, anharmonic ro-vibrational wave functions of diatomic molecules and the corresponding geometry-dependent molecular polarisability invariants computed over the varying internuclear distance using standard *ab initio* methods coupled with response theory [21–27]. Accurate ro-vibrational wave functions of diatomic molecules are obtained by numerical solution to the radial nuclear problem given by Equation (7). These quantities allow us to evaluate numerically the integral in Equation (2) in order to compute the transition matrix element for a specific transition. In the next step, we construct approximations to the distance-dependent polarisability invariants by constructing their Taylor expansions at the internuclear distance corresponding to the ground ro-vibrational state in Equation (3) and truncating them at some low order. Such simplified polarisability invariants representations are subsequently used in the spirit of original Placzek approach to determine the Raman intensities using the integral in Equation (2). Further, we analyse the role of an accurate representation of the ro-vibrational wave functions for the computation of the integral in Equation (2), comparing the Raman intensities computed with accurate anharmonic ro-vibrational wave functions with those computed using the corresponding harmonic ro-vibrational wave functions.

The current study relies to a large degree on the knowledge of accurate potential energy curves used to determine numerically the vibrational wave functions of

diatomic molecules. In particular, the underlying potential energy curve for the molecular hydrogen, being one of the pillars of the current analysis, is known to high accuracy owing to the extensive work of the late Professor Lutosław Wolniewicz. He devoted many decades of his life for producing more and more accurate and physically exact potential energy curves for H₂ and its isotopologues. With this publication we would like to pay a tribute to the memory of Professor Wolniewicz, without whose magnificent work the present analysis could not be adequately performed.

2. Analysis scheme

2.1. Overview

Two components are required for accurate evaluation of the integral in Equation (2) for diatomic molecules: (a) polarisability and (b) ro-vibrational wave functions, both expressed as a function of the internuclear distance. In this section, we define the necessary terms relevant to the present analysis.

Polarizability tensor defined in the Cartesian coordinates consists of two non-vanishing principal components, α_{\perp} , defined as the component perpendicular to the molecular axis, and α_{\parallel} , defined as the component parallel to the molecular axis. For freely rotating molecules, two rotational invariants of polarisability are employed instead: mean polarisability $\bar{\alpha} = (2\alpha_{\perp} + \alpha_{\parallel})/3$ and polarisability anisotropy $\gamma = \alpha_{\parallel} - \alpha_{\perp}$.

Due to the simple structure of diatomic molecules, their accurate ro-vibrational wave functions can be expressed as functions of a single variable, the internuclear distance (r). The ro-vibrational wave functions are determined by numerical solution to the radial nuclear problem given by Equation (7). Each ro-vibrational function obtained in this way is indexed with the vibrational quantum number ν and a rotational quantum number J , and—for our convenience pertaining to the numerical integration procedure used here—also by the span of the internuclear distances over which the function is non-negligible.

In order to generate reliable reference data for testing the double harmonic approximation usually used for computing Raman intensities,³ we start by evaluating the integral in Equation (2) in the most accurate form, i.e. with anharmonic ro-vibrational wave functions ψ^{anhrm} and exact polarisability invariants ($\bar{\alpha}^{\text{exact}}$ or γ^{exact}). Both quantities are computed over a fine grid of internuclear distances and represented as cubic splines. Raman intensity for the fundamental transition is then computed using the relevant transition matrix elements.

This quantity constitutes our reference against which the approximate forms of the same quantity are compared.

In the next step, we construct approximate forms of the quantities needed to evaluate the integral in Equation (2), namely, sets of harmonic wave functions ψ^{harmonic} determined from harmonic potentials and Taylor series expansions of polarisability invariants at the equilibrium internuclear distance, denoted as $\bar{\alpha}^{(n)}$ or $\gamma^{(n)}$, where n refers to the Taylor series expansions truncated at the n^{th} order. The approximate quantities are then used to compute the relevant matrix elements, and finally the corresponding Raman intensities.

We conclude our analysis by performing a detailed comparison between the exact and approximate sets of Raman intensities of the studied diatomic molecules and present a discussion of accuracy of the studied approximations.

2.2. Computational details

2.2.1. Polarizability calculations

Static (frequency-independent) components of the polarisability tensor were computed over a fine grid of internuclear distances for all the studied molecules using various *ab initio* techniques. Specific details for each molecule are given below.

Distance-dependent static polarisabilities of H₂, HD and D₂ were adapted from our earlier work [28]. In brief, the polarisability was computed using CCSD technique [29,30] (equivalent in this case to FCI calculations) using a composite basis set comprising of hydrogen's atomic *aug-mcc-pV6Z* basis set of Mielke et al. [31] downloaded from the EMSL basis set database [32,33] and custom designed bond-functions. These calculations were performed using DALTON quantum chemistry package [30]. In the case of H₂, HD and D₂, a large discrepancy in the values of mean polarisability and its anisotropy were observed when using standard atomic-basis in comparison with the results computed using explicitly correlated wave functions by Rychlewski [21–23]. The application of standard AO basis in conjunction with additional bond-functions placed at five equidistant positions along the internuclear axis resulted in significantly improved polarisabilities, comparable in quality to the explicitly correlated results of Rychlewski. The additional bond functions comprised of even-tempered Gaussian primitives (*8s6p*), constructed using the expression $\alpha\beta^{1-k}$ with $\alpha = 1.8518519$ and $\beta = 3$ for the *s*-functions and with $\alpha = 2.520$ and $\beta = 3$ for the *p*-functions. The detailed development of this composite basis set was described in our earlier work [28]. The previously presented results filled up gaps in the available data relevant to the spectroscopy

of molecular hydrogen, and resolved several irregularities in the polarisability datasets reported by Rychlewski [22].

The polarisabilities for the remaining molecules studied here (HF, HCl, CO, N₂ and F₂) were initially computed using response theory with the coupled cluster with single, double and perturbative triple excitations (CCSD(T)) wave functions [34,35] and the *aug-cc-pVQZ* basis sets [36,37]. The cfour quantum chemistry package was used for these computations [38,39]. Keeping in mind the development for the molecular hydrogen described above, it was natural to expect that additional bond functions placed along the internuclear axis would systematically improve the computed polarisabilities also for HF, HCl, CO, N₂ and F₂. Unfortunately, this was not the case. The gradually developed bond-functions (for more details, see Section S2 of the supplementary material) allowed us to systematically improve the total energy values for these molecules, but at the same time the observed changes in the polarisability invariants displayed rather unsystematic and at times unexpected convergence patterns with no apparent trends. Consequently, we gave up the idea of using composite basis sets and decided to use the CCSD(T)/*aug-cc-pVQZ* polarisabilities in our analysis.

Some of the distance-dependent CCSD(T)/*aug-cc-pVQZ* polarisability components α_{\perp} and α_{\parallel} for the non-hydrogen systems showed rather peculiar behaviour at larger internuclear distances. To avoid the possibility of using systematically erroneous polarisability data in our analysis, stemming from the inadequate description of electronic structure of these molecules with CCSD(T), we computed the values of α_{\perp} and α_{\parallel} using also other methods, including Hartree-Fock (HF) [27,40], complete active space self-consistent field (CASSCF) [41–45], density functional theory (DFT) [46–49] and occasionally coupled cluster with single, double, and triple excitations (CCSDT) [38,50–52] methodologies. These results showed rather surprising lack of internal consistency; we discuss them in detail separately in Section 3.1.1. Here we only briefly mention that the HF, CASSCF, and DFT calculations were performed using the *aug-cc-pVQZ* [36,37] basis sets on the DALTON quantum chemistry package [30]. The CASSCF calculations used the following sequence of valence active spaces: (8e, 5o) for HF, (8e, 5o) for HCl, (10e, 8o) for CO, (10e, 8o) for N₂, and (14e, 8o) for F₂. The DFT calculations were performed using the B3LYP functional [53–56]. The CCSDT computations were performed in the same manner as those with CCSD(T), but using a smaller basis set (*aug-cc-pVTZ*) [36,37]. All basis sets used in this work were obtained from the EMSL basis set database [32,33].

2.2.2. Wavefunctions

The ro-vibrational wave functions $\psi_{v,J} \equiv \psi_{v,J}(r)$ for the studied diatomic molecules were obtained by numerically solving the radial nuclear equation

$$\left[\frac{-1}{2\mu r^2} \frac{\partial}{\partial r} r^2 \frac{\partial}{\partial r} + \frac{J(J+1)}{2\mu r^2} + V(r) \right] \psi_{v,J}(r) = E_{v,J} \psi_{v,J}(r) \quad (7)$$

where the potential energy curve $V(r)$ was adapted from earlier works or determined in a way described below using reported sets of experimental transition frequencies.

The potential energy curves for molecular hydrogen and its isotopologues were adapted from the work of Wolniewicz [57] who reported the Born-Oppenheimer potential together with the scaled adiabatic, relativistic, and radiative corrections to it. Each of these components was interpolated to a finer grid spanning the interval from 0.2 to 12.0 a.u. and combined together in order to obtain the final potential energy curve. These curves were given an analytic, third-order spline representations, which was subsequently used in numerical solution to the radial nuclear Schrödinger problem. For details, see our previous work [28].

The usual way of determining accurate potentials $V(r)$ for solving radial nuclear Schrödinger problem is based on quantum chemical calculations. Here, however, we resorted to a different solution, which can be referred to as an inverse Schrödinger problem. To this end, we employed a set of accurate experimental ro-vibrational levels and transition frequencies to determine the best potential energy curve that reproduces these levels and frequencies via the solution to Equation (7). There are many possible choices of the analytical form for the potential energy function that can be used in this context. Here, for the HF, DF, HCl, DCl, N₂, ¹⁴N¹⁵N, and F₂ molecules, we chose the modified Morse function [58,59]

$$V(r) = \alpha \left[1 - e^{-c_0(r-r_e)+c_1(r-r_e)^2+c_2(r-r_e)^3} \right]^2 \quad (8)$$

with five fitting parameters α , c_0 , c_1 , c_2 , and r_e and for CO and ¹³C¹⁶O, we used the Rydberg function [60–62]

$$V(r) = D_e \left[1 - [1 + b(r - r_e)] e^{-b(r - r_e)} \right] \quad (9)$$

with $b = \sqrt{\frac{k_e}{D_e}}$ and with three fitting parameters k_e , D_e , and r_e . The optimal values of the parameters for each potential energy function were obtained by performing a non-linear least squares optimisation with experimental ro-vibrational transition frequencies and energy levels covering $v = 0-3$ and $J = 0-4$ used as reference. The

optimised parameters are tabulated in Table 1. A detailed description of the optimisation procedure, along with the list of experimental ro-vibrational levels used in the optimisation and the corresponding values obtained by solving the ro-vibrational Schrödinger equation with the fitted potentials, are given in Section S3 of supplementary material.

A similar approach was used to determine the corresponding harmonic wave functions ψ^{harm} . The only difference to the just discussed scheme used for finding accurate ro-vibrational wave functions ψ^{anharm} concerned using a set of harmonic energy levels for each molecule as a reference and an analytical potential expression $V(r) = k(r - r_e)^2$ with r_e corresponding to the equilibrium internuclear distance with the force constant k optimised to reproduce the harmonic vibrational frequency ω_e of each system. The values of r_e and ω_e were taken from the compilation of Herzberg and Huber [63]. The values of these constants together with the reproduced harmonic levels are given in Section S4 of supplementary material.

The solution to the radial nuclear Schrödinger equation in Equation (7) was constructed numerically using the collocation method [64,65] with the five-point stencil representations of the derivative operators. The Hamiltonian matrix was diagonalised for each rotational state J separately. A detailed process of constructing the Hamiltonian matrix and its diagonalisation is described in detail in Section S4 of the supplementary material. The resulting ro-vibrational wave functions $\psi_{v,J}$ were determined only on the collocation grid and their analytical representation was subsequently obtained as a third-order spline. The relevant scheme for solution of Equation (7) was implemented in Python using NumPy [66,67].

The spline representations [68] of the computed polarisability invariants $\Omega = \bar{\alpha}, \gamma$ and the resulting ro-vibrational wave functions $\psi_{v,J}$ were subsequently used in an adaptive Gauss-Kronrod-Patterson quadrature [69–71] to compute numerically the integral in Equation (10) yielding the required transition matrix elements

$$\langle \psi_{v',J'} | \Omega | \psi_{v,J} \rangle = \int_{r_{\min}}^{r_{\max}} \psi_{v',J'} \Omega \psi_{v,J} r^2 dr \quad (10)$$

The lower and upper integration limits, r_{\min} and r_{\max} , respectively, were selected in such a way that both the involved ro-vibrational wave functions $\psi_{v,J}$ and $\psi_{v',J'}$ were negligible ($|\psi_{v,J}|, |\psi_{v',J'}| < 10^{-6}$) beyond the interval $[r_{\min}, r_{\max}]$.

The integral in Equation (10) can be used for computing the normalisation of each ro-vibrational wave function if we set $\Omega = 1$. We use this condition to determine

Table 1. Details regarding the potential energy curve for the studied molecules in this work. For hydrogen and its isotopologues, we adapt the potential energy curve from the work of Wolniewicz (Ref. [57]) after cubic-spline interpolation (Ref. [28]). For the other molecules, the optimised parameters of the analytical potential functions used are listed (see text for more details).

Molecule	Type	Parameters	Molecule	Type	Parameters
H ₂		Ref. [28,57]	CO	Rydberg	$D_e = 0.37563416$
HD		Ref. [28,57]			$k_e = 1.22186557$
D ₂		Ref. [28,57]			$r_e = 2.13081292$
HF	Morse	$\alpha = 0.35329865$	¹³ C ¹⁶ O	Rydberg	$D_e = 0.37416296$
		$c_0 = 0.93760569$			$k_e = 1.2221096$
		$c_1 = 0.16211304$			$r_e = 2.13237061$
		$c_2 = -0.02953036$	N ₂	Morse	$\alpha = 0.44320257$
		$r_e = 1.73219245$			$c_0 = 1.28992997$
DF	Morse	$\alpha = 0.32449615$			$c_1 = c_2 = 0^a$
		$c_0 = 0.93760569$			$r_e = 2.07375152$
		$c_1 = 0.15017749$	¹⁴ N ¹⁵ N	Morse	$\alpha = 0.71696534$
		$c_2 = -0.0334324$			$c_0 = 1.00934466$
		$r_e = 1.73163182$			$c_1 = c_2 = 0^a$
HCl	Morse	$\alpha = 0.19657065$			$r_e = 2.07636687$
		$c_0 = 0.91807751$	F ₂	Morse	$\alpha = 0.07997099$
		$c_1 = c_2 = 0^a$			$c_0 = 1.37680336$
		$r_e = 2.4121016$			$c_1 = c_2 = 0^a$
DCl	Morse	$\alpha = 0.19581078$			$r_e = 2.66708039$
		$c_0 = 0.92009524$			
		$c_1 = c_2 = 0^a$			
		$r_e = 2.41109861$			

^a The parameter c_0 was sufficient to reproduce the observed energy levels in this case, and hence, c_1 and c_2 were set to zero.

the normalisation constants for each of the used here ro-vibrational wave functions, so in the following equations and discussions all the normalisation constants will be automatically equal to one and omitted. For interested reader, we mention that all those wave functions are available from GitHub [72] repository; for details, see Section 6.

2.2.3. Truncated expansions of polarisability invariants

Truncated Taylor series approximations of polarisability invariants at the internuclear distance $r_0 = \langle \psi_{v=0, J=0} | r | \psi_{v=0, J=0} \rangle$ were constructed as follows:

- The values of $\Omega = \bar{\alpha}, \gamma$ computed on the original grid were fitted over the interval $[r_{\min}, r_{\max}]$ using a nine-degree polynomial. We used typically 50–60 grid points for this step. The resulting polynomial was represented in a Taylor-series-like form

$$\Omega = \sum_{n=0}^9 \frac{\Omega_{r_0}^{(n)}}{n!} (r - r_0)^n \quad (11)$$

where $\Omega_{r_0}^{(n)}$ can be interpreted as the n^{th} order derivative of Ω at r_0 . The fit reproduced Ω^{exact} faithfully with typical deviations of around 1×10^{-4} ($\leq 0.1\%$).

- Only Ω^{exact} and $\Omega^{(1)}$ were used to compute the matrix elements of the polarisability invariants in conjunction with the exact anharmonic wave functions ψ^{anharm} or their harmonic approximations ψ^{harmn} . Squares of these matrix elements are tabulated in Tables 2, 3, and 4.

3. Results

The present analysis relies to a large degree on accurate, distance-dependent polarisabilities and ro-vibrational wave functions as the necessary ingredients. Therefore, we start our discussion by presenting the computed perpendicular and parallel components of the polarisability tensor for each molecule together with the corresponding rotational invariants. These results are followed by a short discussion of the ro-vibrational wave functions and a compilation of the computed matrix elements and the resulting Raman intensities.

3.1. Polarizabilities

The distance-dependent polarisability components (α_{\perp} and α_{\parallel}) and the associated invariants ($\bar{\alpha}$ and γ) for molecular hydrogen are shown in Figure 1. These results, adapted from our previous work [28], were found to be in good agreement with the analogous results computed

Table 2. Comparison of the matrix elements of polarisability invariants and the total Raman intensity^a for the fundamental vibrational transition $|v = 1, J = 0\rangle \leftarrow |v = 0, J = 0\rangle$ for molecular hydrogen and its isotopologues computed using CCSD methodology, and with exact anharmonic wave functions (ψ^{anhrm}) or their harmonic counterparts (ψ^{harmn}), along with exact polarisability invariants ($\bar{\alpha}^{\text{exact}}$ and γ^{exact}) or their linear approximations ($\bar{\alpha}^{(1)}$ and $\gamma^{(1)}$).

Mean polarisability $\langle \psi_{v=0, J=0} \bar{\alpha} \psi_{v=1, J=0} \rangle^2$			
	H ₂	HD	D ₂
$\psi = \psi^{\text{anhrm}}, \bar{\alpha} = \bar{\alpha}^{\text{exact}}$	0.5468	0.4699	0.3801
$\psi = \psi^{\text{harmn}}, \bar{\alpha} = \bar{\alpha}^{\text{exact}}$	0.5075 (−7.2 %)	0.4402 (−6.3 %)	0.3601 (−5.3 %)
$\psi = \psi^{\text{anhrm}}, \bar{\alpha} = \bar{\alpha}^{(1)}$	0.5430 (−0.7 %)	0.4668 (−0.7 %)	0.3778 (−0.6 %)
$\psi = \psi^{\text{harmn}}, \bar{\alpha} = \bar{\alpha}^{(1)}$	0.5322 (−2.7 %)	0.4587 (−2.4 %)	0.3724 (−2.0 %)
Polarizability anisotropy $\langle \psi_{v=0, J=0} \gamma \psi_{v=1, J=0} \rangle^2$			
	H ₂	HD	D ₂
$\psi = \psi^{\text{anhrm}}, \gamma = \gamma^{\text{exact}}$	0.3740	0.3165	0.2514
$\psi = \psi^{\text{harmn}}, \gamma = \gamma^{\text{exact}}$	0.3114 (−16.7 %)	0.2697 (−14.8 %)	0.2203 (−12.3 %)
$\psi = \psi^{\text{anhrm}}, \gamma = \gamma^{(1)}$	0.3528 (−5.6 %)	0.3006 (−5.0 %)	0.2407 (−4.2 %)
$\psi = \psi^{\text{harmn}}, \gamma = \gamma^{(1)}$	0.3458 (−7.5 %)	0.2954 (−6.7 %)	0.2372 (−5.6 %)
Total Raman intensity $\langle \psi_{v=0, J=0} \bar{\alpha} \psi_{v=1, J=0} \rangle^2 + \frac{7}{45} \langle \psi_{v=0, J=0} \gamma \psi_{v=1, J=0} \rangle^2$			
	H ₂	HD	D ₂
$\psi = \psi^{\text{anhrm}}, \bar{\alpha} = \bar{\alpha}^{\text{exact}}, \gamma = \gamma^{\text{exact}}$	0.6049	0.5191	0.4192
$\psi = \psi^{\text{harmn}}, \bar{\alpha} = \bar{\alpha}^{\text{exact}}, \gamma = \gamma^{\text{exact}}$	0.5559 (−8.1 %)	0.4822 (−7.1 %)	0.3944 (−5.9 %)
$\psi = \psi^{\text{anhrm}}, \bar{\alpha} = \bar{\alpha}^{(1)}, \gamma = \gamma^{(1)}$	0.5979 (−1.2 %)	0.5135 (−1.1 %)	0.4153 (−0.9 %)
$\psi = \psi^{\text{harmn}}, \bar{\alpha} = \bar{\alpha}^{(1)}, \gamma = \gamma^{(1)}$	0.5860 (−3.1 %)	0.5046 (−2.8 %)	0.4093 (−2.4 %)

^aCorresponding to linearly polarised excitation and parallelly and perpendicularly polarised detection scheme, usually denoted in literature as (incident_{||}, detection_{||+⊥}).

Table 3. Comparison of matrix elements of mean polarisability for the fundamental vibrational transition $|v = 1, J = 0\rangle \leftarrow |v = 0, J = 0\rangle$ for nine diatomic molecules, computed at various levels of theory (HF, CASSCF, DFT and CCSD(T)) and approximations: with exact anharmonic ro-vibrational wave functions (ψ^{anhrm}) or their harmonic counterparts (ψ^{harmn}), and with exact mean polarisability ($\bar{\alpha}^{\text{exact}}$) or its linear approximation ($\bar{\alpha}^{(1)}$).

Mean polarisability $\langle \psi_{v=0, J=0} \bar{\alpha} \psi_{v=1, J=0} \rangle^2$										
Method	Components	HF	DF	HCl	DCl	CO	¹³ C ¹⁶ O	N ₂	¹⁴ N ¹⁵ N	F ₂
HF	$\psi = \psi^{\text{anhrm}}, \bar{\alpha} = \bar{\alpha}^{\text{exact}}$	0.1118	0.0782	0.3824	0.2653	0.1100	0.1074	0.1914	0.1885	0.2617
	$\psi = \psi^{\text{anhrm}}, \bar{\alpha} = \bar{\alpha}^{(1)}$	0.1062	0.0754	0.3656	0.2568	0.1094	0.1069	0.1908	0.1882	0.2585
		(−5.0%)	(−3.6%)	(−4.4%)	(−3.2%)	(−0.5%)	(−0.5%)	(−0.3%)	(−0.2%)	(−1.2%)
CASSCF	$\psi = \psi^{\text{anhrm}}, \bar{\alpha} = \bar{\alpha}^{\text{exact}}$	0.1349	0.0939	0.3084	0.2162	0.1149	0.1123	0.1222	0.1204	0.0169
	$\psi = \psi^{\text{anhrm}}, \bar{\alpha} = \bar{\alpha}^{(1)}$	0.1271	0.0899	0.3014	0.2120	0.1143	0.1116	0.1223	0.1206	0.0184
		(−5.8%)	(−4.3%)	(−2.3%)	(−1.9%)	(−0.5%)	(−0.6%)	(+0.1%)	(+0.2%)	(+8.6%)
DFT	$\psi = \psi^{\text{anhrm}}, \bar{\alpha} = \bar{\alpha}^{\text{exact}}$	0.1266	0.0895	0.3665	0.2567	0.1051	0.1027	0.1485	0.1463	0.1085
	$\psi = \psi^{\text{anhrm}}, \bar{\alpha} = \bar{\alpha}^{(1)}$	0.1229	0.0876	0.3568	0.2517	0.1045	0.1021	0.1483	0.1462	0.1086
		(−2.9%)	(−2.1%)	(−2.7%)	(−1.9%)	(−0.6%)	(−0.6%)	(−0.1%)	(−0.1%)	(+0.1%)
CCSD(T)	$\psi = \psi^{\text{anhrm}}, \bar{\alpha} = \bar{\alpha}^{\text{exact}}$	0.1392	0.0979	0.3842	0.2694	0.1254	0.1226	0.1161	0.1144	0.0523
	$\psi = \psi^{\text{anhrm}}, \bar{\alpha} = \bar{\alpha}^{(1)}$	0.1353	0.0923	0.3753	0.2648	0.1248	0.1220	0.1165	0.1149	0.0554
		(−2.8%)	(−5.7%)	(−2.3%)	(−1.7%)	(−0.5%)	(−0.5%)	(+0.4%)	(+0.4%)	(+5.9%)
	$\psi = \psi^{\text{harmn}}, \bar{\alpha} = \bar{\alpha}^{(1)}$	0.1328	0.0911	0.3687	0.2614	0.1240	0.1212	0.1158	0.1139	0.0548
		(−4.6%)	(−6.9%)	(−4.0%)	(−3.0%)	(−1.1%)	(−1.1%)	(−0.2%)	(−0.4%)	(+4.7%)

using explicitly correlated wave functions by Rychlewski [22]; for more details, see [28]. The computed polarisability tensor components of molecular hydrogen at large internuclear distances converge properly to the correct atomic limit equal to twice of the atomic polarisability of hydrogen [73].

For the other studied here molecules (HF, HCl, CO, N₂, and F₂) the analogous results are shown in Figures 2

and 3. Since the electronic wave functions were computed under the Born-Oppenheimer approximation, the resulting polarisabilities are the same for pairs of isotopologues: HF and DF, HCl and DCl, CO and ¹³C¹⁶O, and N₂ and ¹⁴N¹⁵N. No accurate reference data is available for these molecules in literature, so to be on the safe side we used various quantum chemical methods to verify the correctness of the presented here results. In the

Table 4. Comparison of matrix elements of polarisability anisotropy for the fundamental vibrational transition $|v = 1, J = 0\rangle \leftarrow |v = 0, J = 0\rangle$ for nine diatomic molecules, computed at various levels of theory (HF, CASSCF, DFT and CCSD(T)) and approximations: with exact anharmonic ro-vibrational wave functions (ψ^{anhrm}) or their harmonic counterparts (ψ^{harhm}), and with exact polarisability anisotropy (γ^{exact}) or its linear approximation ($\gamma^{(1)}$).

		Polarisability anisotropy $\langle \psi_{v=0, J=0} \gamma \psi_{v=1, J=0} \rangle^2$								
Method	Components	HF	DF	HCl	DCI	CO	$^{13}\text{C}^{16}\text{O}$	N_2	$^{14}\text{N}^{15}\text{N}$	F_2
HF	$\psi = \psi^{\text{anhrm}}, \gamma = \gamma^{\text{exact}}$	0.3470	0.2391	1.5021	1.0335	0.1962	0.1917	0.2419	0.2382	1.7744
	$\psi = \psi^{\text{anhrm}}, \gamma = \gamma^{(1)}$	0.3215	0.2262	1.4166	0.9910	0.1945	0.1901	0.2404	0.2371	1.7481
	$\psi = \psi^{\text{harhm}}, \gamma = \gamma^{(1)}$	0.3157	0.2234	1.3917	0.9785	0.1932	0.1889	0.2389	0.2351	1.7281
		(-7.4%)	(-5.4%)	(-5.7%)	(-4.1%)	(-0.9%)	(-0.9%)	(-0.6%)	(-0.5%)	(-1.5%)
		(-9.0%)	(-6.6%)	(-7.3%)	(-5.3%)	(-1.5%)	(-1.5%)	(-1.2%)	(-1.3%)	(-2.6%)
CASSCF	$\psi = \psi^{\text{anhrm}}, \gamma = \gamma^{\text{exact}}$	0.4802	0.3299	1.2631	0.8797	0.2358	0.2303	0.1512	0.1489	0.0290
	$\psi = \psi^{\text{anhrm}}, \gamma = \gamma^{(1)}$	0.4426	0.3108	1.2235	0.8569	0.2332	0.2258	0.1507	0.1486	0.0345
	$\psi = \psi^{\text{harhm}}, \gamma = \gamma^{(1)}$	0.4346	0.3069	1.2021	0.8460	0.2317	0.2244	0.1497	0.1474	0.0341
		(-7.8%)	(-5.8%)	(-3.1%)	(-2.6%)	(-1.1%)	(-2.0%)	(-0.4%)	(-0.2%)	(+18.9%)
		(-9.5%)	(-7.0%)	(-4.8%)	(-3.8%)	(-1.7%)	(-2.6%)	(-1.0%)	(-1.1%)	(+17.5%)
DFT	$\psi = \psi^{\text{anhrm}}, \gamma = \gamma^{\text{exact}}$	0.3295	0.2296	1.2790	0.8873	0.2525	0.2467	0.2158	0.2126	0.5318
	$\psi = \psi^{\text{anhrm}}, \gamma = \gamma^{(1)}$	0.3124	0.2209	1.2269	0.8611	0.2505	0.2448	0.2148	0.2119	0.5301
	$\psi = \psi^{\text{harhm}}, \gamma = \gamma^{(1)}$	0.3068	0.2181	1.2053	0.8501	0.2488	0.2432	0.2135	0.2102	0.5240
		(-5.2%)	(-3.8%)	(-4.1%)	(-3.0%)	(-0.8%)	(-0.8%)	(-0.5%)	(-0.3%)	(-0.3%)
		(-6.9%)	(-5.0%)	(-5.8%)	(-4.2%)	(-1.5%)	(-1.4%)	(-1.1%)	(-1.2%)	(-1.5%)
CCSD(T)	$\psi = \psi^{\text{anhrm}}, \gamma = \gamma^{\text{exact}}$	0.3448	0.2379	1.2490	0.8672	0.3008	0.2939	0.1286	0.1267	0.1657
	$\psi = \psi^{\text{anhrm}}, \gamma = \gamma^{(1)}$	0.3244	0.2200	1.2009	0.8429	0.2983	0.2912	0.1291	0.1273	0.1802
	$\psi = \psi^{\text{harhm}}, \gamma = \gamma^{(1)}$	0.3185	0.2173	1.1798	0.8321	0.2963	0.2894	0.1283	0.1262	0.1781
		(-5.9%)	(-7.5%)	(-3.9%)	(-2.8%)	(-0.9%)	(-0.9%)	(+0.4%)	(+0.4%)	(+8.7%)
		(-7.6%)	(-8.7%)	(-5.5%)	(-4.0%)	(-1.5%)	(-1.5%)	(-0.2%)	(-0.4%)	(+7.5%)

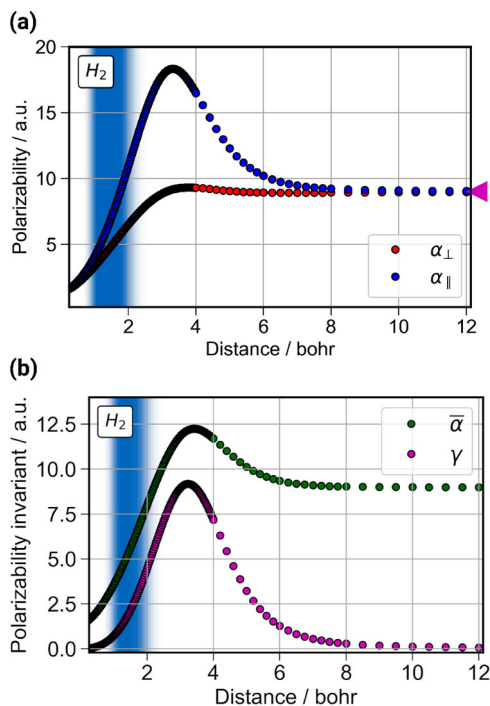


Figure 1. Static (wavelength independent) values of: (a) the polarisability components α_{\perp} and α_{\parallel} , and (b) the associated invariants $\bar{\alpha}$ and γ , plotted as a function of the internuclear distance. These values were calculated using CCSD methodology and the custom designed composite basis (*aug-cc-mccPV6Z* with $5 \times (8s6p)$ bond functions). The region corresponding to the non-negligible values of the vibrational wave functions with $v = 0, 1$ is represented by a blue shade, with the depth of the colour representing the magnitudes of the wave functions. The purple triangle represents separated atom limit equal to $2 \times \alpha(H)$.

case of α_{\perp} , the results obtained using HF, CASSCF, DFT, CCSD(T) and (at times) CCSDT show similar trends in the interval $[r_{\min}, r_{\max}]$, with the values increasing gradually with increasing internuclear distances. We conclude that the computed values of α_{\perp} can be considered as reliable, but their accuracy cannot be expected to be larger than a few percent as substantial numerical discrepancies between curves obtained with various methods suggest.

In the case of α_{\parallel} , the situation is much more serious. In principle, the curves computed with various *ab initio* methods for CO, HF, N_2 , and HCl show similar trends and resemble each other, except maybe for the internuclear distances close to r_{\max} , where the discrepancies between the curves are larger. However, for F_2 , considerable deviations between the computed curves are observed inside almost the whole interval $[r_{\min}, r_{\max}]$, with particularly large discrepancies at larger internuclear distances. This should not be surprising as a similar observation was reported previously by Maroulis [74], who studied the distance-dependent polarisability and hyper-polarisabilities of F_2 using different *ab initio* techniques. From our perspective, however, of the planned analysis of Raman intensities, this is a rather unexpected and unforeseen obstacle, as it is difficult to say without further analysis which of these curves are correct. To resolve this issue we decided to look deeper into this problem by studying the distance dependence of α_{\parallel} and α_{\perp} at the full range of internuclear separations. The results of this investigation are presented in the next section.

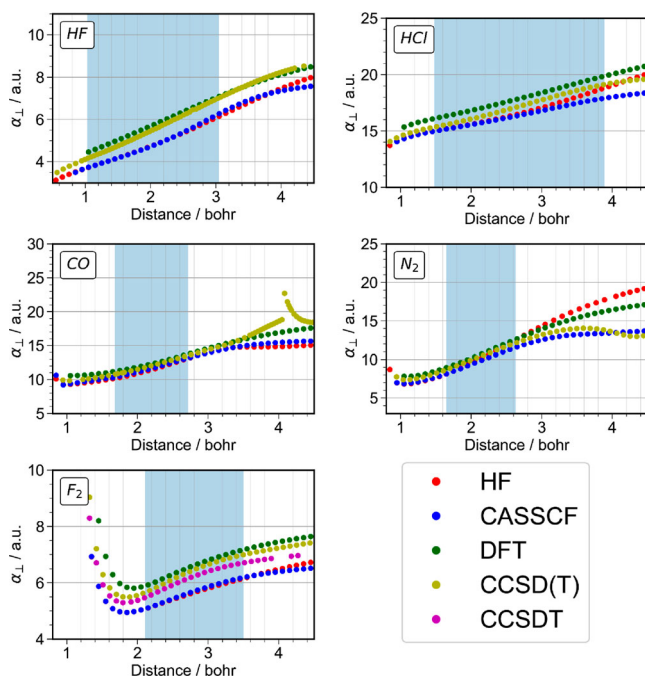


Figure 2. Static (wavelength independent) values of the α_{\perp} component of the polarisability tensor plotted as a function of the internuclear distance calculated using different *ab initio* techniques. The interval spanned by the first vibrational wave function is represented by the blue shaded region in each panel.

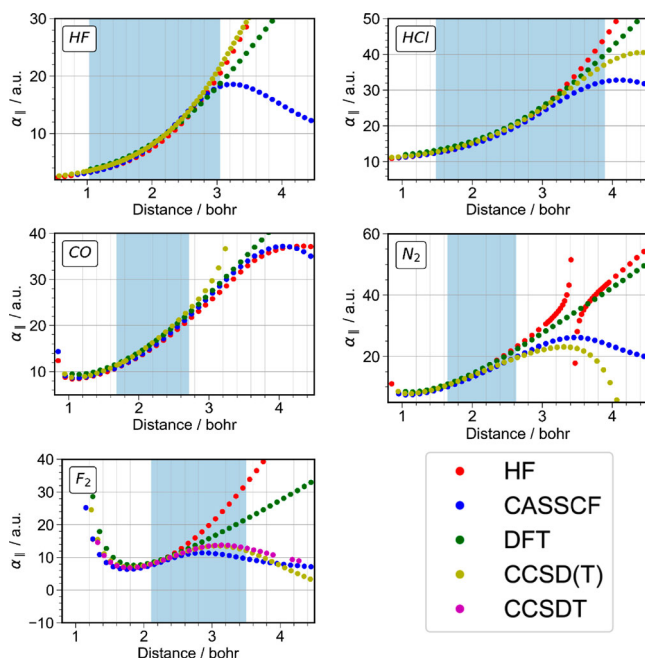


Figure 3. Static (wavelength independent) values of the α_{\parallel} component of the polarisability tensor plotted as a function of the internuclear distance calculated using different *ab initio* techniques. The interval spanned by the first vibrational wave function is represented by the blue shaded region in each panel.

3.1.1. Sanity check for the computed distance-dependent polarisabilities

The values of α_{\parallel} and α_{\perp} computed over larger range of internuclear distances (from 1.2 to 7 bohr) are shown in Figure 4 for all the studied here molecules except molecular hydrogen. At large distances, the values of both components of molecular polarisability should converge to the corresponding atomic limit equal to the sum of atomic polarisabilities. These limits, computed from accurate atomic data [73], are depicted in Figure 4 using purple triangles located at the right edge of each panel. Obviously, most of the used here methods are single-reference in nature and cannot describe adequately the process of molecular dissociation. Therefore, we do not expect that the curves computed with these methods (HF, DFT, and CCSD(T)) would converge to the correct limits. The question we try to address here is rather when these methods loose their applicability and start diverging.

Rather surprisingly, we discovered that α_{\perp} computed with all the tested here *ab initio* methods converge—more or less accurately—to the expected atomic limit. In case of CCSD(T), the calculations for CO and N₂ cannot converge for internuclear separations larger than 4.6 bohr, but even so, the values of α_{\perp} at 4.6 bohr are close to the corresponding atomic limits. The situation is completely different for α_{\parallel} . Practically all the tested here single-reference *ab initio* methods diverge away from the atomic limits, but the trend of divergence is quite different for each method.

The only method which passes our sanity check is CASSCF. Again, this is not surprising, as CASSCF with valence active space is capable of producing correct wave functions over the whole range of internuclear separations, and consequently reproducing physically meaningful values of both components of the polarisability tensor, which converge to the correct atomic limit. Unfortunately, despite of quite reasonable distance dependence of α_{\parallel} and α_{\perp} computed with CASSCF, we proceed rather cautiously with accepting the CASSCF values in our analysis of Raman intensities, because the CASSCF polarisabilities seem to differ from more accurate CCSD(T) and DFT values at distances where all the methods are applicable. The best example can be inferred from Figure 2, where α_{\perp} of F₂ computed with CASSCF and HF differ from the values obtained with other methods by 5–15%. We believe that reliable distance-dependent polarisabilities of many-electron systems—and consequently also reliable Raman intensities of such systems—can be computed only using multireference correlated methods, but the appropriate response theory tools are not yet available.

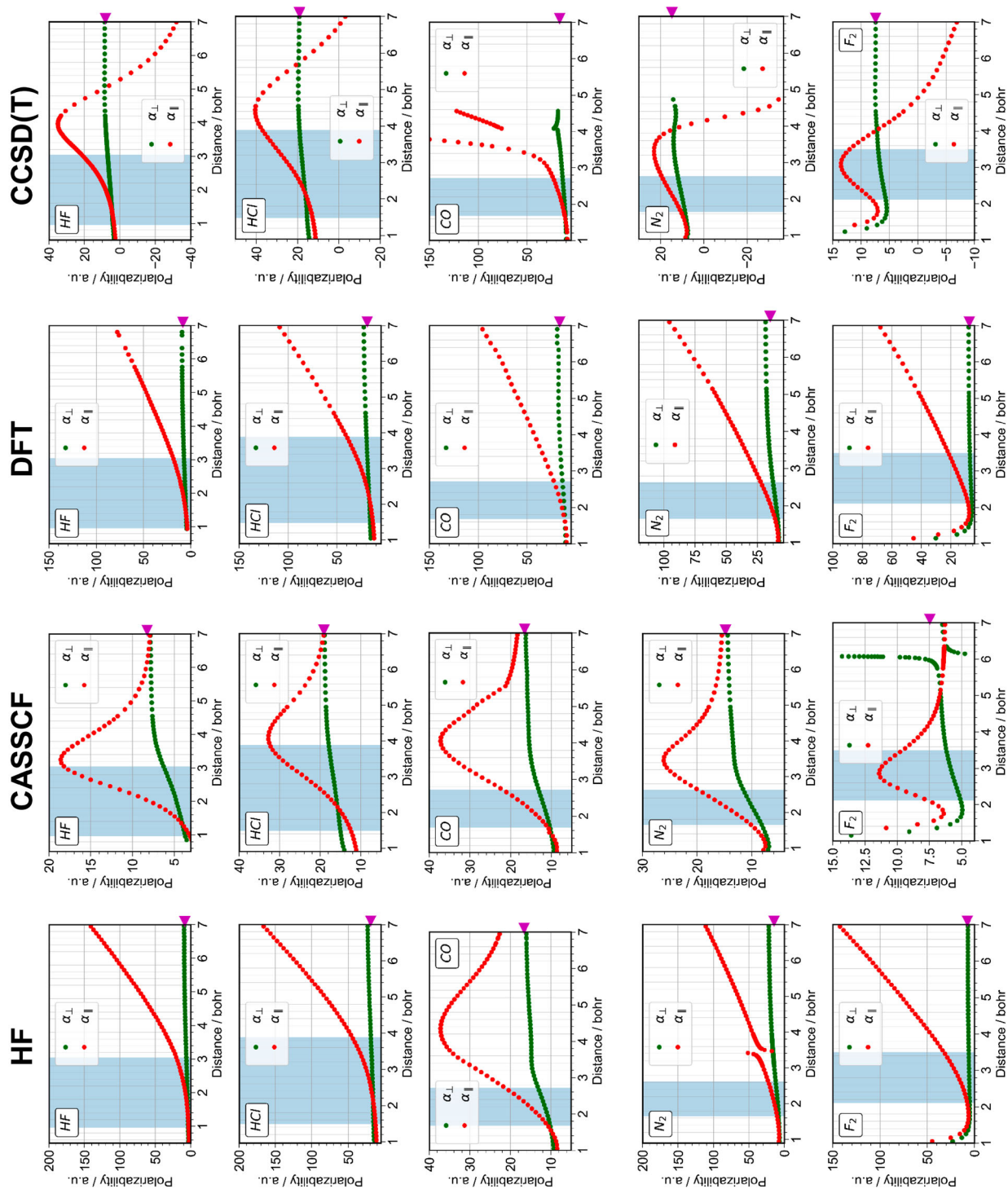


Figure 4. Static (wavelength independent) values of the two components of polarisability (α_{\parallel} and α_{\perp}) for HF, HCl, CO, N_2 , and F_2 plotted as a function of the internuclear distance calculated using different *ab initio* techniques. The interval spanned by the first vibrational wave function is represented by the blue shaded region in each panel. The purple triangle on the right y axes represents the sum of atomic polarisabilities of the constituent atoms.

We are forced to use in our further analysis the CASSCF values of the polarisability tensor invariants as the reference data even if we know that these values are not too accurate. A comparison of results obtained with

other methods is presented later, in Section 3.4, where we use the CASSCF results as a reference and try to estimate the deviations in the total Raman intensities obtained with other *ab initio* techniques.

For some molecules, we observe spiky local features (α_{\parallel} of N_2 at 3.5 bohr with the HF method and α_{\perp} of F_2 at 6.0 bohr with the CASSCF method) or discontinuities (α_{\parallel} and α_{\perp} of CO at 4.1 bohr with the CCSD(T) method) in the computed polarisabilities in Figures 2–4. These originate from the shortcomings of response theory at stretched geometries. Fortunately, all of these spurious features are quite local and do not affect the polarisabilities in the region important for our analysis.

3.2. Ro-vibrational wave functions

Ro-vibrational wave functions ψ^{anharm} for H_2 , HD and D_2 were obtained by a numerical solution of the radial nuclear equation with accurate potential energy functions determined by Wolniewicz [57]. The computed energy levels of ro-vibrational states are compared with accurate experimental and theoretical results in Section S4 of supplementary material. This comparison shows deviations within one wavenumber.

For the other molecules studied in this work, no potential energy curves have been reported in literature that would allow to achieve similar accuracy in the determination of ro-vibrational wave functions ψ^{anharm} . Therefore, to circumvent this difficulty we decided to use an alternative solution that can be referred to as the inverse Schrödinger problem, in which accurate experimental ro-vibrational transition frequencies reported in literature were used to find an optimal shape of the potential energy surface allowing to reproduce these values with best fidelity; more details are given in Section 2.2.2. All the ro-vibrational energy levels computed with this procedure together with all the relevant transition frequencies were found to be within one wavenumber from the reference values. Detailed list of these energy levels and the corresponding transition frequencies is given in Section S4 of supplementary material together with their comparisons to experimental reference data.

3.3. Matrix elements of polarisability invariants and total Raman intensities

The results for H_2 , HD and D_2 are shown in Table 2. We tabulate three different properties: mean polarisability $\langle \psi_{v=0, J=0} | \bar{\alpha} | \psi_{v=1, J=0} \rangle^2$ matrix elements, polarisability anisotropy $\langle \psi_{v=0, J=0} | \gamma | \psi_{v=1, J=0} \rangle^2$ matrix elements, and total Raman intensities $\langle \psi_{v=0, J=0} | \bar{\alpha} | \psi_{v=1, J=0} \rangle^2 + \frac{7}{45} \langle \psi_{v=0, J=0} | \gamma | \psi_{v=1, J=0} \rangle^2$, all computed with four different approaches, in which the ro-vibrational wave function is selected either as ψ^{anharm} or ψ^{harmn} and the polarisability invariants are taken in the exact form ($\bar{\alpha}^{\text{exact}}$ and γ^{exact}) or as its linear approximations ($\bar{\alpha}^{(1)}$ and $\gamma^{(1)}$). Note that the total Raman intensity formula given above

corresponds to linearly polarised excitation and parallelly and perpendicularly polarised detection scheme, usually denoted in literature as (incident $_{\parallel}$, detection $_{\parallel+\perp}$).

The following conclusions can be drawn:

- (1) All the approximations, either pertaining to the simplifications in the ro-vibrational wave functions or to the simplifications in the polarisability tensor invariants, invariably lead to reducing of the values of the computed matrix elements. This eventually results in reduced total Raman intensities with respect to the exact values. This effect is more pronounced when the exact ro-vibrational wave function is replaced by its harmonic approximation (error of 6–8%). Approximating the exact polarisability by its linear form gives smaller error of about 1%.
- (2) The deviations from the exact results in the matrix elements of polarisability anisotropy are always a few times larger than analogous deviations in the matrix elements of mean polarisability, for all types of approximations.
- (3) The largest deviation (16%) in the computed matrix elements is observed for the polarisability anisotropy of H_2 computed by combining harmonic wave function ψ^{harmn} with exact form of the invariant. Surprisingly, using linear approximation to polarisability anisotropy reduces this deviation by about half, owing to error cancellations.
- (4) The deviations in Raman intensities are comparable to those observed for the matrix elements of mean polarisability, due to the fact that the contribution from the polarisability anisotropy matrix elements—laden with substantially larger deviations—is diluted by a small prefactor of 7/45.
- (5) The double harmonic approximation, corresponding to the choice of ψ^{harmn} and $\bar{\alpha}^{(1)}$ and $\gamma^{(1)}$ in the integral in Equation (10), gives an overall error of around 2–3% in the computed Raman intensities. The deviation is slightly smaller for heavier isotopologues of molecular hydrogen.

We have analysed the data for molecular hydrogen separately above, because these results are not affected by possible large systematic errors in the determination of the polarisability invariants used to compute the Raman intensities. We believe that the results for molecular hydrogen are very close to the exact quantum mechanical limit. The results for other molecules discussed below use quite approximate values of the polarisability tensor components as discussed earlier in Section 2.2.1. The effect of the double harmonic approximation can be still approximately assessed using these CASSCF invariants, but the absolute values of the resulting Raman intensities should

Table 5. Comparison of the total Raman intensity for the fundamental vibrational transition $|v = 1, J = 0\rangle \leftarrow |v = 0, J = 0\rangle$ for nine diatomic molecules computed at various levels of theory (HF, CASSCF, DFT and CCSD(T)) and approximations: with exact anharmonic wave functions (ψ^{anharm}) or their harmonic counterparts (ψ^{harmon}), along with exact polarisability invariants ($\bar{\alpha}^{\text{exact}}$ and γ^{exact}) or their linear approximations ($\bar{\alpha}^{(1)}$ and $\gamma^{(1)}$).

		Total Raman intensity = $\langle \psi_{v=0, J=0} \bar{\alpha} \psi_{v=1, J=0} \rangle^2 + \frac{7}{45} \langle \psi_{v=0, J=0} \gamma \psi_{v=1, J=0} \rangle^2$								
Method	Components	HF	DF	HCl	DCI	CO	$^{13}\text{C}^{16}\text{O}$	N_2	$^{14}\text{N}^{15}\text{N}$	F_2
SCF	$\psi = \psi^{\text{anharm}}, \bar{\alpha} = \bar{\alpha}^{\text{exact}}, \gamma = \gamma^{\text{exact}}$	0.1658	0.1154	0.6161	0.4261	0.1405	0.1373	0.2290	0.2256	0.5377
	$\psi = \psi^{\text{anharm}}, \bar{\alpha} = \bar{\alpha}^{(1)}, \gamma = \gamma^{(1)}$	0.1562	0.1105	0.5859	0.4110	0.1396	0.1365	0.2282	0.2251	0.5304
	$\psi = \psi^{\text{harmon}}, \bar{\alpha} = \bar{\alpha}^{(1)}, \gamma = \gamma^{(1)}$	0.1534	0.1092	0.5757	0.4058	0.1387	0.1356	0.2268	0.2232	0.5244
		(-5.8%)	(-4.2%)	(-4.9%)	(-3.5%)	(-0.6%)	(-0.6%)	(-0.3%)	(-0.2%)	(-1.4%)
		(-7.5%)	(-5.4%)	(-6.6%)	(-4.8%)	(-1.2%)	(-1.2%)	(-1.0%)	(-1.1%)	(-2.5%)
CASSCF	$\psi = \psi^{\text{anharm}}, \bar{\alpha} = \bar{\alpha}^{\text{exact}}, \gamma = \gamma^{\text{exact}}$	0.2096	0.1452	0.5049	0.3531	0.1516	0.1481	0.1457	0.1436	0.0214
	$\psi = \psi^{\text{anharm}}, \bar{\alpha} = \bar{\alpha}^{(1)}, \gamma = \gamma^{(1)}$	0.1959	0.1383	0.4918	0.3453	0.1505	0.1467	0.1458	0.1437	0.0238
	$\psi = \psi^{\text{harmon}}, \bar{\alpha} = \bar{\alpha}^{(1)}, \gamma = \gamma^{(1)}$	0.1924	0.1365	0.4831	0.3409	0.1496	0.1458	0.1449	0.1425	0.0235
		(-7.0%)	(-5.1%)	(-2.7%)	(-2.2%)	(-0.7%)	(-1.0%)	(+0.0%)	(+0.1%)	(+9.7%)
		(-8.2%)	(-6.0%)	(-4.3%)	(-3.4%)	(-1.3%)	(-1.6%)	(-0.6%)	(-0.7%)	(+9.5%)
DFT	$\psi = \psi^{\text{anharm}}, \bar{\alpha} = \bar{\alpha}^{\text{exact}}, \gamma = \gamma^{\text{exact}}$	0.1778	0.1252	0.5655	0.3947	0.1443	0.1410	0.1821	0.1794	0.1912
	$\psi = \psi^{\text{anharm}}, \bar{\alpha} = \bar{\alpha}^{(1)}, \gamma = \gamma^{(1)}$	0.1715	0.1220	0.5476	0.3856	0.1434	0.1402	0.1817	0.1792	0.1911
	$\psi = \psi^{\text{harmon}}, \bar{\alpha} = \bar{\alpha}^{(1)}, \gamma = \gamma^{(1)}$	0.1684	0.1205	0.5380	0.3807	0.1425	0.1393	0.1806	0.1777	0.1889
		(-3.6%)	(-2.6%)	(-3.2%)	(-2.3%)	(-0.6%)	(-0.6%)	(-0.2%)	(-0.1%)	(-0.1%)
		(-5.3%)	(-3.8%)	(-4.9%)	(-3.5%)	(-1.3%)	(-1.2%)	(-0.8%)	(-0.9%)	(-1.2%)
CCSD(T)	$\psi = \psi^{\text{anharm}}, \bar{\alpha} = \bar{\alpha}^{\text{exact}}, \gamma = \gamma^{\text{exact}}$	0.1928	0.1349	0.5785	0.4043	0.1722	0.1683	0.1361	0.1341	0.0781
	$\psi = \psi^{\text{anharm}}, \bar{\alpha} = \bar{\alpha}^{(1)}, \gamma = \gamma^{(1)}$	0.1857	0.1265	0.5621	0.3959	0.1712	0.1673	0.1366	0.1347	0.0834
	$\psi = \psi^{\text{harmon}}, \bar{\alpha} = \bar{\alpha}^{(1)}, \gamma = \gamma^{(1)}$	0.1824	0.1249	0.5523	0.3909	0.1701	0.1663	0.1358	0.1335	0.0825
		(-3.7%)	(-6.2%)	(-2.8%)	(-2.1%)	(-0.6%)	(-0.6%)	(+0.4%)	(+0.4%)	(+6.9%)
		(-5.4%)	(-7.4%)	(-4.5%)	(-3.3%)	(-1.2%)	(-1.2%)	(-0.2%)	(-0.4%)	(+5.6%)

be treated with caution. We hope that more accurate means of determination of distance-dependent polarisability invariants will be available soon and these numerical results can be rectified in this way.

The results for HF, DF, HCl, DCI, CO, $^{13}\text{C}^{16}\text{O}$, N_2 , $^{14}\text{N}^{15}\text{N}$, and F_2 are presented in Table 3 (mean polarisability matrix elements), Table 4 (polarizability anisotropy matrix elements), and Table 5 (total Raman intensities). This time, the results are computed with three different approaches: (a) the exact approach with ψ^{anharm} and $\bar{\alpha}^{\text{exact}}$ and γ^{exact} , (b) single harmonic approximation with ψ^{anharm} and $\bar{\alpha}^{(1)}$ and $\gamma^{(1)}$, and (c) doubly harmonic approximation with ψ^{harmon} and $\bar{\alpha}^{(1)}$ and $\gamma^{(1)}$. The following discussion is based on the CASSCF results, but for completeness, Tables 3–5 contain data computed also with other methods (HF, DFT, and CCSD(T)). These results are discussed later in Section 3.5.

From the CASSCF data in Tables 3–5, the following conclusions can be drawn:

- (1) In a close analogy to molecular hydrogen, the matrix elements of polarisability anisotropy are affected by the harmonic approximations to a larger degree than the matrix elements of mean polarisability. This observation concerns all of the studied molecules, with larger deviations detected for lighter molecules.
- (2) Within a pair of isotopologues (i.e. HF and DF, HCl and DCI, CO and $^{13}\text{C}^{16}\text{O}$, N_2 and $^{14}\text{N}^{15}\text{N}$), the deviations between the matrix element computed using

the exact polarisability invariants and the matrix element computed using approximate polarisability invariants are similar, despite that the matrix elements for both for isotopologues may differ to a large degree. This is not surprising since the pairs of isotopologues share the same polarisability invariants. Consequently, similar observation concerns also the total Raman intensities of isotopologues.

- (3) In the interval $[r_{\text{min}}, r_{\text{max}}]$, corresponding to the non-negligible values of the ro-vibrational wave functions, the differences between the exact polarisability invariants ($\bar{\alpha}^{(\text{exact})}$ and $\gamma^{(\text{exact})}$) and their linear approximants ($\bar{\alpha}^{(1)}$ and $\gamma^{(1)}$) are rather small for all of the studied molecules except F_2 , for which the shape of both the invariants resembles a convex hull in this region. Consequently, $\bar{\alpha}^{(1)}$ and particularly $\gamma^{(1)}$ are bad approximations to $\bar{\alpha}^{(\text{exact})}$ and $\gamma^{(\text{exact})}$, respectively, which results in large deviations between the exact and approximate matrix elements of polarisability invariants and the resulting total Raman intensities. (For a relevant comparison between F_2 and N_2 , see Figure 5.)
- (4) The deviations from the exact results caused by the double harmonic approximation—corresponding to the choice of ψ^{harmon} and $\bar{\alpha}^{(1)}$ and $\gamma^{(1)}$ in the integral in Equation (10)—are molecule dependent and range between -7.5% and $+7.5\%$ for the $\bar{\alpha}$ matrix elements, between -9.5% and $+17.5\%$ for the γ matrix elements, and between -8.2% and $+9.5\%$ for the total Raman intensities. The deviations are

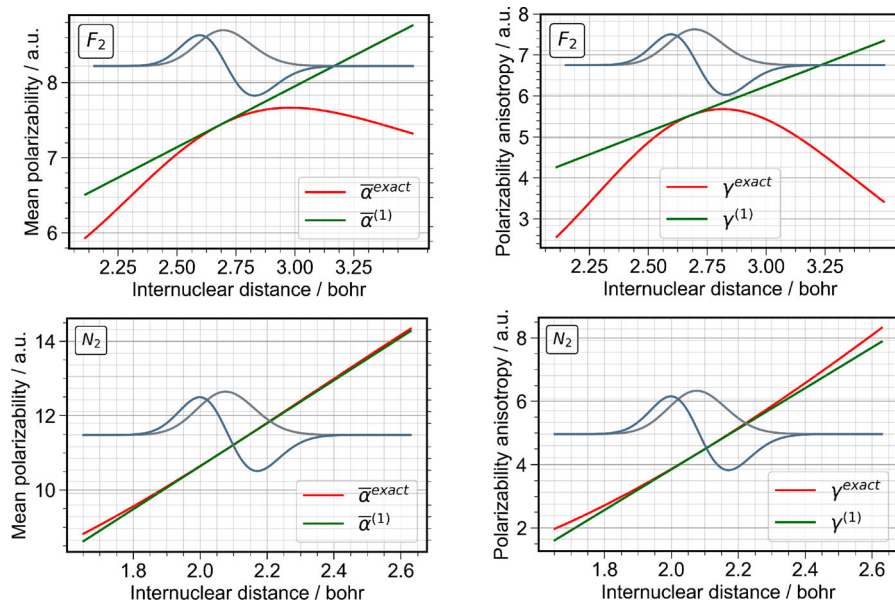


Figure 5. A comparison between $\bar{\alpha}^{\text{exact}}$ and $\bar{\alpha}^{(1)}$ (left panels) and between γ^{exact} and $\gamma^{(1)}$ (right panels) for F_2 (upper panels) and N_2 (lower panels), together with the relevant vibrational wave functions $\psi_{v=0, J=0}^{\text{exact}}$ and $\psi_{v=1, J=0}^{\text{exact}}$ depicted in the background in grey to illustrate the extent of the integration region in the integral in Equation (10). It is clear that for N_2 , the exact polarisability tensor invariants $\bar{\alpha}^{\text{exact}}$ and γ^{exact} are well modelled by their linear approximants $\bar{\alpha}^{(1)}$ and $\gamma^{(1)}$, while for F_2 , such an approximation leads to significant errors. The polarisability invariants are computed using CASSCF.

slightly smaller for the heavier isotopologue within a given pair of isotopologues.

- (5) The accuracy of the single harmonic approximation is 30–40% better than the accuracy of the double harmonic approximation. An exception for this rule is F_2 , for which both approximations are very bad (error of $> 17\%$ for γ and $> 7\%$ for $\bar{\alpha}$). Typical errors attributed to the harmonic approximations are close to several percents.

3.4. Uncertainties arising from inconsistencies in the quantum chemical description of polarisability invariants

In Section 3.1.1 we have demonstrated that the distance-dependent polarisability tensor components α_{\parallel} and α_{\perp} computed with various *ab initio* techniques can differ substantially due to the insufficient description of the electronic wave functions in the vicinity of the dissociation limit by the single-reference-based methods; for details, see Figure 4. The discrepancies between the computed curves are sizable even in the integration interval $[r_{\text{min}}, r_{\text{max}}]$ relevant to Equation (10), where the four tested *ab initio* techniques display considerable disparities (for details, see Figures 2 and 3). It is not surprising that the polarisability matrix elements computed with those curves and tabulated in Tables 3 and 4 differ substantially and affect the resulting Raman intensities tabulated in Table 5. Consequently, large differences in

the values of the total Raman intensities computed with different theoretical methods (HF, CASSCF, DFT and CCSD(T)) are observed.

A few regularities (and irregularities) are worth highlighting:

- (1) The polarisability invariants matrix elements computed with the exact methodology with various *ab initio* techniques may differ substantially. For HF, HCl, CO, and N_2 and their isotopologues, the detected differences can be as large as 56% for the mean polarisability and 60% for the polarisability anisotropy; both these maximal deviations are observed between the matrix elements of N_2 derived from the CASSCF and Hartree-Fock polarisabilities.
- (2) These maximal deviations have been determined without taking into account the F_2 molecule, for which the deviations are enormous: the matrix elements determined using the Hartree-Fock polarisability invariants are over 15 times larger ($\bar{\alpha}$) and over 60 larger (γ) than the corresponding CASSCF quantities, while for DFT and CCSD(T) these factors are approximately 6 and 18 times larger, and 3 and 6 times larger, respectively.
- (3) To understand the strong dependence of the computed matrix elements and the total Raman intensities of F_2 on the selected *ab initio* technique, we have plotted in Figure 6 a close-up view of the distance-dependent polarisability invariants $\bar{\alpha}^{\text{exact}}$ and γ^{exact}

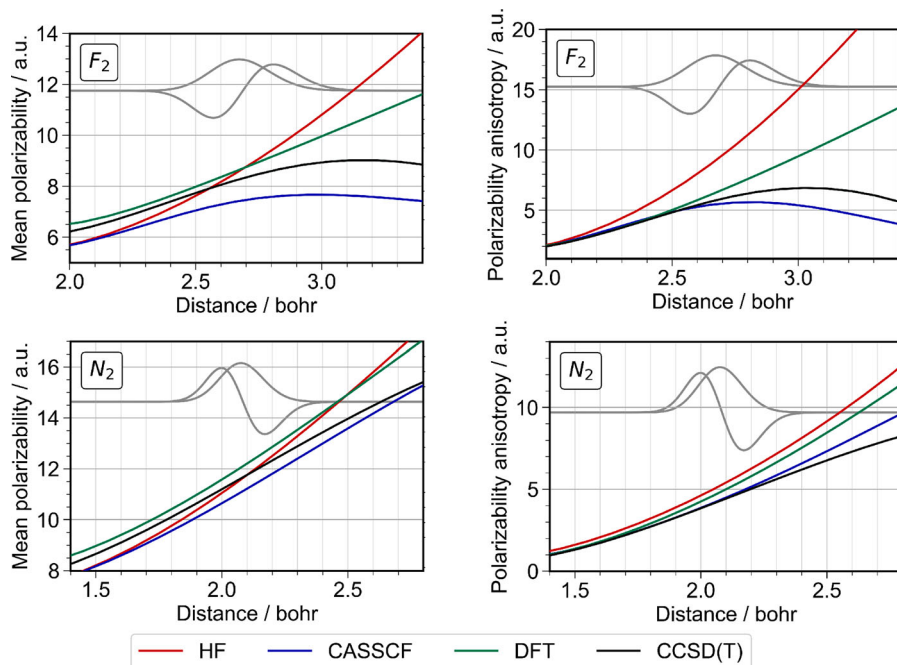


Figure 6. A comparison between distance-dependent polarisability invariants $\bar{\alpha}^{\text{exact}}$ (left panels) and γ^{exact} (right panels) for F_2 (upper panels) and N_2 (lower panels) computed with various *ab initio* methods, together with the relevant vibrational wave functions $\psi_{v=0, J=0}^{\text{exact}}$ and $\psi_{v=1, J=0}^{\text{exact}}$ depicted in the background in grey to illustrate the extent of the integration region in the integral in Equation (10). It is clear that for N_2 , all the methods produce curves that can be approximated by linear functions with similar slopes, while for F_2 , distinct functional dependence of curves obtained with different methods causes large differences in the computed matrix elements and total Raman intensities.

computed with various methods for F_2 and N_2 . The difference between these two molecules is striking. For N_2 , all the curves inside the integration interval $[r_{\min}, r_{\max}]$ could be reasonably well approximated by linear functions with similar slopes. For F_2 , similar operation could be performed only for the DFT and HF curves, while the curves computed with both CASSCF and CCSD(T) have strong quadratic character. This observations explains well why F_2 behaves differently than other molecules.

- (4) There seem to be no obvious correlation between the method of calculations, the molecule under study, and the magnitude and the direction of the deviation from the CASSCF results. For every molecule and for every method, the deviations can be either small or large and either positive or negative.
- (5) Within a pair of isotopologues (i.e. HF and DF, HCl and DCl, CO and $^{13}\text{C}^{16}\text{O}$, $\text{N}_2\text{N } 2$ and $^{14}\text{N}^{15}\text{N}$), the deviations between the matrix elements computed with various *ab initio* techniques display similar trends. Similar observation concerns also the total Raman intensities of isotopologues.

The deviations from CASSCF in the matrix elements computed with DFT, HF, and CCSD(T) automatically propagate to the associated deviations in the total Raman

intensities. These deviations are illustrated graphically in Figure 7, where for each pair of isotopologues, we have represented the CASSCF total Raman intensity as a blue bar of height 100 and the total Raman intensities computed with other *ab initio* methods as bars in other colours, each of a height associated with the relevant total Raman intensity corresponding to a given method.

The most important observations concerning these results can be summarised as follows:

- (1) For HF, HCl, CO, and N_2 and their isotopologues, the difference between the reference CASSCF total Raman intensities and analogous results computed with other methods can be quite substantial with deviations from 5% to 57%. For F_2 , the differences are much larger: 264% for CCSD(T), 793% for DFT and over 2000% for HF.
- (2) The deviations associated with using inadequate electronic structure method to compute distance-dependent polarisability invariants completely overshadow the inaccuracies associated with double harmonic approximation. It seems at the moment that solving the problem how to produce accurate distance-dependent polarisability invariants is much more pressing than addressing other methodological

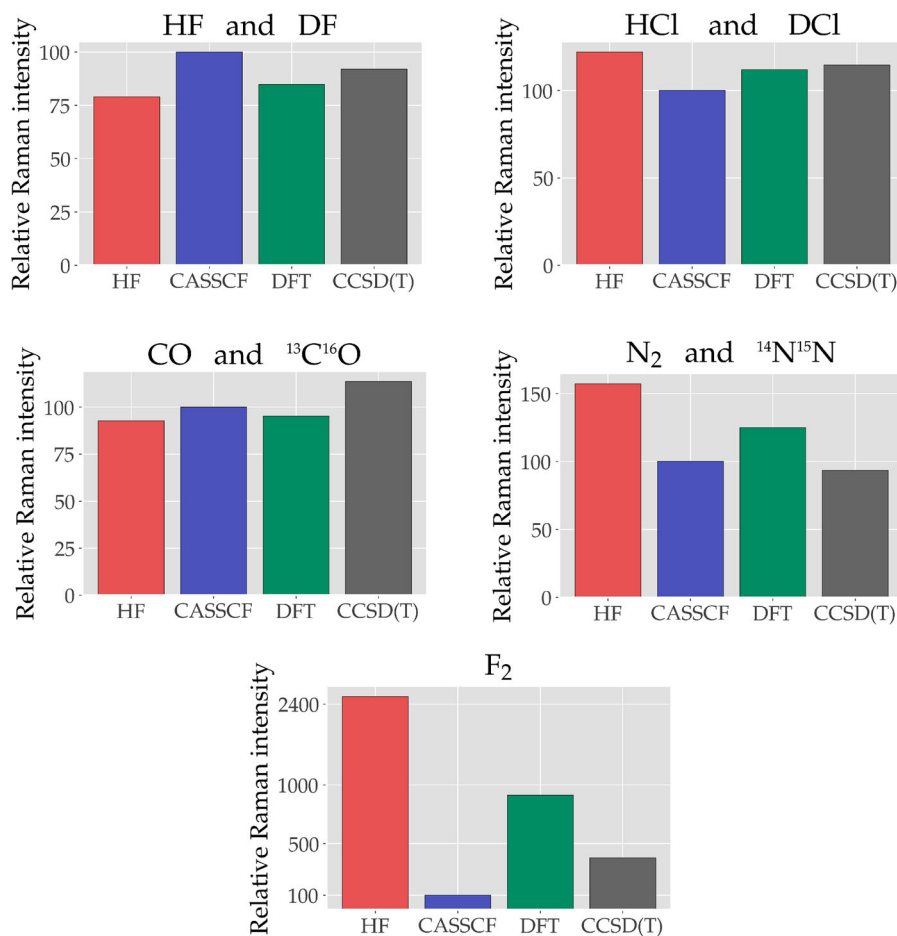


Figure 7. Comparison of the relative Raman intensities of the fundamental vibrational transition computed with various *ab initio* methods for nine studied here diatomic molecules. The matrix elements of polarisability invariants were computed using the $\bar{\alpha}^{\text{exact}}$ and γ^{exact} polarisability invariants determined by different methods and exact wave functions ψ^{anharm} determined from experimental data. Results from other methods are normalised relative to the CASSCF results.

details in the process of determination of accurate total Raman intensities.

3.5. Discussion

The tested here double harmonic approximation is characterised by errors between -8.2% and $+9.5\%$ for the 12 studied molecules. This is not small, because typical experimental errors associated with the acquisition of Raman intensities are lower and could be estimated to be within $\pm 5\%$ [75]. Therefore, precise Raman investigations aiming at accuracy better than 5% should not use double harmonic approximation for the interpretation of the experimental results. An alternative to the standard approach is the scheme presented by us in the current manuscript. However, the actual correspondence between the theoretical off-resonance Raman cross-sections and the experimental Raman intensities is more complicated. The reported here total Raman intensities correspond to the frequency-independent Raman

cross-sections, $(\epsilon_0/\pi)^2 \tilde{\nu}_0^{-1} \tilde{\nu}_s^{-3} \times (d\sigma/d\Omega)$, expressed in atomic units, with $\tilde{\nu}_0$ denoting the absolute frequency of the incident light and $\tilde{\nu}_s$ denoting the absolute frequency of the scattered light [76,77]. A direct comparison of these quantities with experimentally determined Raman cross-sections would involve the inclusion of the frequency factor $\tilde{\nu}_0 \tilde{\nu}_s^3$, which takes into account the information about the specific laser used in the experiment and the particular molecular transition. Moreover, experimental Raman intensities include also the effect of temperature affecting the Boltzmann population of the initial state, and the wavelength-dependent response function of the Raman spectrometer. The first of this quantities is relatively straightforward to account for, while the determination of the correction associated with the wavelength-dependent sensitivity of the Raman spectrometer can be by itself an arduous task [78,79].

In a sense, the accuracy estimates of the double harmonic approximation given in the previous paragraph fulfil the main goal of the current study. However, in

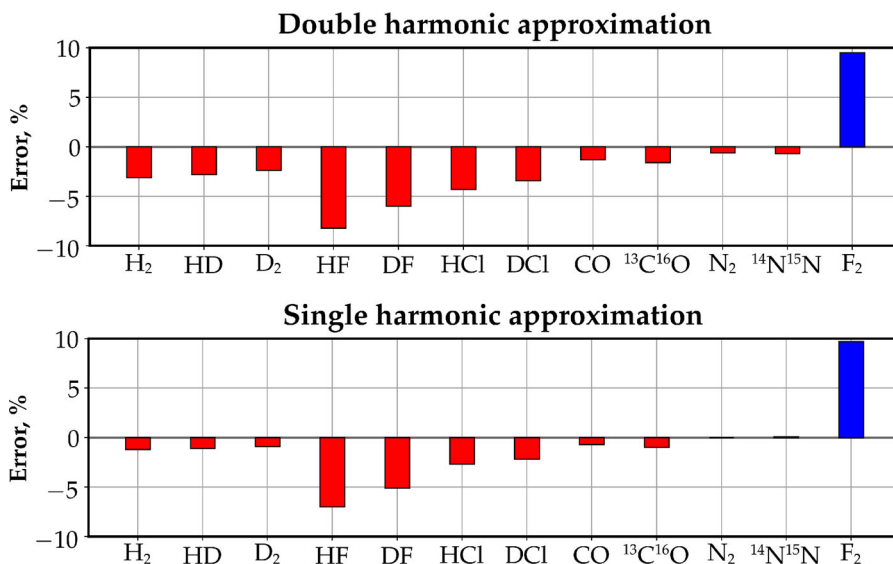


Figure 8. Comparison of errors originating from the double harmonic approximation (upper panel) and the single harmonic approximation (lower panel) in the process of determination of total Raman intensities for the fundamental vibrational transition for 12 diatomic molecules. The errors correspond to the differences between results computed with the exact methodology based on anharmonic ro-vibrational wave functions ψ^{anharm} and distance-dependent polarisability invariants $\bar{\alpha}^{\text{exact}}$ and γ^{exact} , and the approximate results based on the harmonic ro-vibrational wave functions ψ^{harm} and linear approximants $\bar{\alpha}^{(1)}$ and $\gamma^{(1)}$ (double harmonic approximation) or on the anharmonic ro-vibrational wave functions ψ^{anharm} and linear approximants $\bar{\alpha}^{(1)}$ and $\gamma^{(1)}$ (single harmonic approximation).

the process of constructing the answer to the question risen at the beginning of this manuscript, we have realised that there exists much more pressing problem that needs to be urgently addressed in order to provide the physical chemistry community with a method of producing reliable theoretical estimates of total Raman intensities. Namely, we have discovered that the currently available quantum chemical techniques of determination of distance-dependent molecular polarisabilities suffer from serious drawbacks associated with inadequate description of molecular electronic structure at larger internuclear distances. It is well known that single reference methods cannot describe adequately molecules with stretched bonds, which is associated with their inability of a correct description of the dissociation limit. We have discovered here that this limitation affects already the accuracy of molecular polarisability components determined with HF, DFT, and CCSD(T) for molecules with bonds stretched out of the equilibrium position by a relatively small amount. The resulting distance-dependent polarisability components computed using HF, DFT, and CCSD(T) differ significantly from each other and diverge systematically from the correct long-range behaviour. We have circumvented this problem by applying in the current study the CASSCF method to determine the polarisability invariant, because it seems at the moment to be the only method able to correctly

describe the physically sane behaviour of polarisability invariants at the whole range of the internuclear separations relevant in the process of computing total Raman intensities. However, CASSCF does not account for dynamic correlation and consequently, the polarisability components determined in this way are not too accurate. We hope that this explicit demonstration of the problems associated with determination of accurate distance-dependent polarisability components will stimulate the community for finding better and more reliable methods of computing this quantity. In this regard, CASPT2 (second-order complete active space perturbation theory) and NEVPT2 (second-order n -electronic valence state perturbation theory) techniques [27] would be the most promising way of computing physically-meaningful distance-dependent polarisabilities, but at the moment the CASPT2 and NEVPT2 response theory codes are not yet available.

4. Conclusions

We show in this study that the total Raman intensities of fundamental vibrational transitions for 12 diatomic molecules computed within the double harmonic approximation are characterised by errors between -8.2% and $+9.5\%$ with respect to an exact treatment based on anharmonic ro-vibrational wave functions

ψ^{anhrm} and distance-dependent polarisability invariants $\bar{\alpha}^{\text{exact}}$ and γ^{exact} . A graphical compilation of the resulting errors is given in Figure 8 for all the studied here molecules. These errors are slightly larger than the analogous errors originating from the single harmonic approximation. The largest discrepancies are observed for F₂, for which the exact functional dependence of the polarisability invariants $\bar{\alpha}^{\text{exact}}$ and γ^{exact} cannot be well approximated by linear functions $\bar{\alpha}^{(1)}$ and $\gamma^{(1)}$, respectively.

For isotopologues of molecular hydrogen, the reported here values of total Raman intensities should be close to the exact absolute values. The situation is quite different for heavier molecules, HF, DF, HCl, DCl, CO, ¹³C¹⁶O, N₂, ¹⁴N¹⁵N, and F₂, for which we have realised (unexpectedly) that the determination of accurate distance-dependent polarisability invariants needed to evaluate the integral in Equation (2) is difficult if not impossible with the currently existing quantum chemical codes. The spatial extent of the ro-vibrational wave functions requires the knowledge of polarisability invariants at stretched molecular geometries, where the single reference methods start to fail (producing large numerical errors) and the available multireference techniques are not accurate enough (producing likely sizable errors). The errors associated with inaccuracies in the distance-dependent polarisability tensor seem to be much larger than the errors originating from the shortcomings of the harmonic approximations, and at the moment seem to be principal factor determining the accuracy of the computed total Raman intensities. The best example here is the F₂ molecule, for which the total Raman intensities computed with various quantum chemical methods can differ even by a factor of 20 (for details, see Section 3.4 and Figure 7). These findings clearly show that there exist an urgent need for developing more accurate methods of computing the distance-dependent polarisability invariants, applicable also to distorted molecular geometries. We believe that this discovery is the most important outcome of our work.

Notes

1. Total wave function here is expressed as product of harmonic oscillator wave functions of each normal mode, i.e. $\psi_{v_i} = \prod \phi_{v_i}(Q_k)$, and similarly $\psi_{v_f} = \prod \phi_{v_f}(Q_k)$.
2. This approach also covers the infrared intensities where the polarisability operator is replaced by the dipole moment operator.
3. We limit our discussion to the transitions in the ground electronic state which is non-degenerate. Only off-resonance Raman scattering intensities are studied here.

Disclosure statement

No potential conflict of interest was reported by the author(s).

Funding

This work was financially supported by Ministry of Science and Technology of Taiwan [grant numbers 105-2923-M-009-001-MY3, 108-2113-M-009-010-MY3, and 103-2113-M-009-001] and the Center for Emergent Functional Matter Science of National Yang Ming Chiao Tung University from the Featured Areas Research Center Program within the framework of the Higher Education Sprout Project by the Ministry of Education (MOE), Taiwan.

Data availability statement

Online repository at GitHub [72], indexed with DOI (10.5281/zenodo.6126144), contains the following auxiliary data: (i) datasets on the polarisability invariants for H₂, HD, D₂ (generated using the CCSD methodology) and for HF, HCl, CO, N₂, and F₂ (generated using the CASSCF methodology), (ii) the potential energy curves used in the computations of exact and approximate ro-vibrational wave functions, (iii) ro-vibrational wave functions ψ^{anhrm} and ψ^{hrm} for all the studied molecules (including isotopologues) with $v = 0, 1$ and $J = 0, 1, 2, 3$, (iv) python [67,80,81] program implementing the collocation method to produce the ro-vibrational energy levels and wave functions for a given potential, and (v) python program using the collocation method for determination of an optimal potential energy curve reproducing a given dataset of experimental ro-vibrational energies and transition frequencies.

ORCID

Ankit Raj  <http://orcid.org/0000-0002-2495-3354>

Henryk A. Witek  <http://orcid.org/0000-0002-9013-1287>

References

- [1] G. Placzek, *Handb. Radiol. Akad. Verlagsgessellschaft VI* **2**, 209–374 (1934).
- [2] E.B. Wilson, J.C. Decius and P.C. Cross, *Molecular Vibrations: The Theory of Infrared and Raman Vibrational Spectra* (Dover Publications, New York, 1955).
- [3] B.A. Hess, L.J. Schaad, P. Carsky and R. Zahradnik, *Chem. Rev.* **86**, 709–730 (1986). doi:10.1021/cr00074a004
- [4] M.D. Halls, J. Velkovski and H.B. Schlegel, *Theor. Chem. Acc.* **105**, 413–421 (2001). doi:10.1007/s002140000204
- [5] A.P. Scott and L. Radom, *J. Phys. Chem.* **100**, 16502–16513 (1996). doi:10.1021/jp960976r
- [6] K.K. Irikura, R.D. Johnson and R.N. Kacker, *J. Phys. Chem. A* **109**, 8430–8437 (2005). doi:10.1021/jp052793n
- [7] NIST Standard Reference Database 101, CCCBD: Pre-computed vibrational scaling factors, NIST <https://cccbdb.nist.gov/vibscalejust.asp>.
- [8] M.W. Wong, *Chem. Phys. Lett.* **256**, 391–399 (1996). doi:10.1016/0009-2614(96)00483-6
- [9] J.P. Merrick, D. Moran and L. Radom, *J. Phys. Chem. A* **111**, 11683–11700 (2007). doi:10.1021/jp073974n

- [10] R.D. Johnson, K.K. Irikura, R.N. Kacker and R. Kessel, *J. Chem. Theory Comput.* **6**, 2822–2828 (2010). doi:10.1021/ct100244d
- [11] D.O. Kashinski, G.M. Chase, R.G. Nelson, O.E.D. Nallo, A.N. Scales, D.L. VanderLey and E.F.C. Byrd, *J. Phys. Chem. A* **121**, 2265–2273 (2017). doi:10.1021/acs.jpca.6b12147
- [12] H.K. Dhah, Ph.D. Dissertation, University of Tennessee Knoxville, TN, USA, 2018.
- [13] Y. Cornaton, M. Ringholm, O. Louant and K. Ruud, *Phys. Chem. Chem. Phys.* **18** (5), 4201–4215 (2016). doi:10.1039/C5CP06657C
- [14] R. Herman and R.F. Wallis, *J. Chem. Phys.* **23**, 637–646 (1955). doi:10.1063/1.1742069
- [15] T.C. James and W. Klemperer, *J. Chem. Phys.* **31**, 2664–2669 (1959). doi:10.1063/1.1730279
- [16] C. Asawaroengchai and G.M. Rosenblatt, *J. Chem. Phys.* **72**, 2664–2669 (1980). doi:10.1063/1.439412
- [17] H. Hamaguchi, I. Suzuki and A.D. Buckingham, *Mol. Phys.* **43**, 963–973 (2006). doi:10.1080/00268978100101791
- [18] H. Hamaguchi, A.D. Buckingham and W.J. Jones, *Mol. Phys.* **43**, 1311–1319 (2006). doi:10.1080/00268978100102081
- [19] H. Hamaguchi, A.D. Buckingham and W.J. Jones, *Mol. Phys.* **46**, 1093–1098 (2006). doi:10.1080/00268978200101821
- [20] A. Raj, H.A. Witek and H. Hamaguchi, *Mol. Phys.* **118**, e1632950 (2019). doi:10.1080/00268976.2019.1632950
- [21] J. Rychlewski, *Mol. Phys.* **41**, 833–842 (2006). doi:10.1080/00268978000103191
- [22] J. Rychlewski, *Chem. Phys. Lett.* **73**, 135–138 (1980). doi:10.1016/0009-2614(80)85220-1
- [23] J. Rychlewski, *J. Chem. Phys.* **78**, 7252–7259 (1983). doi:10.1063/1.444713
- [24] H. Ågren, O. Vahtras and B. Minaev, *Adv. Quantum Chem.* **27**, 71–162 (1996). doi:10.1016/S0065-3276(08)60251-8
- [25] P. Jørgensen, H.J.A. Jensen and J. Olsen, *J. Chem. Phys.* **89**, 3654–3661 (1988). doi:10.1063/1.454885
- [26] J. Olsen, D.L. Yeager and P. Jørgensen, *J. Chem. Phys.* **91**, 381–388 (1989). doi:10.1063/1.457471
- [27] T. Helgaker, P. Jørgensen and J. Olsen, *Molecular Electronic-Structure Theory* (John Wiley & Sons, New York, 2000).
- [28] A. Raj, H. Hamaguchi and H.A. Witek, *J. Chem. Phys.* **148**, 104308 (2018). doi:10.1063/1.5011433
- [29] O. Christiansen, A. Halkier, H. Koch, P. Jørgensen and T. Helgaker, *J. Chem. Phys.* **108**, 2801–2816 (1998). doi:10.1063/1.475671
- [30] K. Aidas, C. Angeli, K.L. Bak, V. Bakken, R. Bast, L. Boman, O. Christiansen, R. Cimiraglia, S. Coriani, P. Dahle, E.K. Dalskov, U. Ekström, T. Enevoldsen, J.J. Eriksen, P. Ettenhuber, B. Fernández, L. Ferrighi, H. Fliegl, L. Frediani, K. Hald, A. Halkier, C. Hättig, H. Heiberg, T. Helgaker, A.C. Hennum, H. Hettema, E. Hjertenaes, S. Høst, I.M. Høyvik, M.F. Iozzi, B. Jansik, H.J.A. Jensen, D. Jonsson, P. Jørgensen, J. Kauczor, S. Kirpekar, T. Kjaergaard, W. Klopper, S. Knecht, R. Kobayashi, H. Koch, J. Kongsted, A. Krapp, K. Kristensen, A. Ligabue, O.B. Lutnaes, J.I. Melo, K.V. Mikkelsen, R.H. Myhre, C. Neiss, C.B. Nielsen, P. Norman, J. Olsen, J.M.H. Olsen, A. Osted, M.J. Packer, F. Pawłowski, T.B. Pedersen, P.F. Provasi, S. Reine, Z. Rinkevicius, T.A. Ruden, K. Ruud, V.V. Rybkin, P. Sałek, C.C.M. Samson, A.S. de Merás, T. Saue, S.P.A. Sauer, B. Schimmelpfennig, K. Sneskov, A.H. Steindal, K.O. Sylvester-Hvid, P.R. Taylor, A.M. Teale, E.I. Tellgren, D.P. Tew, A.J. Thorvaldsen, L. Thøgersen, O. Vahtras, M.A. Watson, D.J.D. Wilson, M. Ziolkowski and H. Ågren, *Wiley Interdiscip. Rev.: Comput. Mol. Sci.* **4**, 269–284 (2013). doi:10.1002/wcms.1172
- [31] S.L. Mielke, B.C. Garrett and K.A. Peterson, *J. Chem. Phys.* **116**, 4142–4161 (2002). doi:10.1063/1.1432319
- [32] B.P. Pritchard, D. Altarawy, B. Didier, T.D. Gibson and T.L. Windus, *J. Chem. Inf. Model.* **59**, 4814–4820 (2019). doi:10.1021/acs.jcim.9b00725
- [33] K.L. Schuchardt, B.T. Didier, T. Elsethagen, L. Sun, V. Gurumoorthi, J. Chase, J. Li and T.L. Windus, *J. Chem. Inf. Model.* **47**, 1045–1052 (2007). doi:10.1021/ci600510j
- [34] K. Raghavachari, G.W. Trucks, J.A. Pople and M. Head-Gordon, *Chem. Phys. Lett.* **157**, 479–483 (1989). doi:10.1016/S0009-2614(89)87395-6
- [35] R.J. Bartlett, J. Watts, S. Kucharski and J. Noga, *Chem. Phys. Lett.* **165**, 513–522 (1990). doi:10.1016/0009-2614(90)87031-L
- [36] T.H. Dunning, *J. Chem. Phys.* **90**, 1007–1023 (1989). doi:10.1063/1.456153
- [37] R.A. Kendall, T.H. Dunning and R.J. Harrison, *J. Chem. Phys.* **96**, 6796–6806 (1992). doi:10.1063/1.462569
- [38] D.A. Matthews, L. Cheng, M.E. Harding, F. Lipparini, S. Stopkowitz, T.C. Jagau, P.G. Szalay, J. Gauss and J.F. Stanton, *J. Chem. Phys.* **152**, 214108 (2020). doi:10.1063/5.0004837
- [39] J.F. Stanton, J. Gauss, L. Cheng, M.E. Harding, D.A. Matthews, P.G. Szalay, CFOUR, Coupled-Cluster techniques for Computational Chemistry, a quantum-chemical program package with contributions from A.A. Auer, A. Asthana, R.J. Bartlett, U. Benedikt, C. Berger, D.E. Bernholdt, S. Blaschke, Y.J. Bomble, S. Burger, O. Christiansen, D. Datta, F. Engel, R. Faber, J. Greiner, M. Heckert, O. Heun, M. Hilgenberg, C. Huber, T.-C. Jagau, D. Jonsson, J. Jusélius, T. Kirsch, K. Klein, G.M. Kopper, W.J. Lauderdale, F. Lipparini, J. Liu, T. Metzroth, L.A. Mück, D.P. O'Neill, T. Nottoli, D.R. Price, E. Prochnow, C. Puzzarini, K. Ruud, F. Schiffmann, W. Schwalbach, C. Simmons, S. Stopkowitz, A. Tajti, J. Vázquez, F. Wang and J.D. Watts, the integral packages MOLECULE (J. Almlöf and P.R. Taylor), PROPS (P.R. Taylor), ABACUS (T. Helgaker, H.J. Aa. Jensen, P. Jørgensen, and J. Olsen), and ECP routines by A. V. Mitin and C. van Wüllen, For the current version, see <https://www.cfour.de>.
- [40] D.R. Hartree and W. Hartree, *Proc. R. Soc. London, Ser. A* **150**, 9–33 (1935). doi:10.1098/rspa.1935.0085
- [41] D. Hegarty and M.A. Robb, *Mol. Phys.* **38**, 1795–1812 (1979). doi:10.1080/00268977900102871
- [42] M. Frisch, I.N. Ragazos, M.A. Robb and H.B. Schlegel, *Chem. Phys. Lett.* **189**, 524–528 (1992). doi:10.1016/0009-2614(92)85244-5
- [43] J. Olsen and P. Jørgensen, *J. Chem. Phys.* **82**, 3235–3264 (1985). doi:10.1063/1.448223
- [44] H.J.A. Jensen, P. Jørgensen and H. Ågren, *J. Chem. Phys.* **87**, 451–466 (1987). doi:10.1063/1.453590
- [45] J. Olsen, *Int. J. Quantum Chem.* **111**, 3267–3272 (2011). doi:10.1002/qua.23107

- [46] P. Hohenberg and W. Kohn, *Phys. Rev.* **136**, B864–B871 (1964). doi:10.1103/PhysRev.136.B864
- [47] W. Kohn and L.J. Sham, *Phys. Rev.* **140**, A1133–A1138 (1965). doi:10.1103/PhysRev.140.A1133
- [48] R.G. Parr and W. Yang, *Density-Functional Theory of Atoms and Molecules (International Series of Monographs on Chemistry)* (Oxford University Press, New York, USA, 1994).
- [49] A.D. Becke, *J. Chem. Phys.* **140**, 18A301 (2014). doi:10.1063/1.4869598
- [50] J. Noga and R.J. Bartlett, *J. Chem. Phys.* **86**, 7041–7050 (1987). doi:10.1063/1.452353
- [51] G.E. Scuseria and H.F. Schaefer, *Chem. Phys. Lett.* **152**, 382–386 (1988). doi:10.1016/0009-2614(88)80110-6
- [52] J. Gauss and J.F. Stanton, *Phys. Chem. Chem. Phys.* **2**, 2047–2060 (2000). doi:10.1039/a909820h
- [53] A.D. Becke, *J. Chem. Phys.* **98**, 5648–5652 (1993). doi:10.1063/1.464913
- [54] P.J. Stephens, F.J. Devlin, C.F. Chabalowski and M.J. Frisch, *J. Phys. Chem.* **98**, 11623–11627 (1994). doi:10.1021/j100096a001
- [55] S.H. Vosko, L. Wilk and M. Nusair, *Can. J. Phys.* **58**, 1200–1211 (1980). doi:10.1139/p80-159
- [56] C. Lee, W. Yang and R.G. Parr, *Phys. Rev. B* **37**, 785–789 (1988). doi:10.1103/PhysRevB.37.785
- [57] L. Wolniewicz, *J. Chem. Phys.* **99**, 1851–1868 (1993). doi:10.1063/1.465303
- [58] P.M. Morse, *Phys. Rev.* **34**, 57–64 (1929). doi:10.1103/PhysRev.34.57
- [59] Y.P. Varshni, *Rev. Mod. Phys.* **29**, 664–682 (1957). doi:10.1103/RevModPhys.29.664
- [60] R. Rydberg, *Z. Angew. Phys.* **73**, 376–385 (1932). doi:10.1007%2Fbf01341146
- [61] H.Y. Abdullah, *Bull. Mater. Sci.* **42**, 57 (2019). doi:10.1007/s12034-019-1740-5
- [62] J.P. Araújo and M.Y. Ballester, *Int. J. Quantum Chem.* **121**, e26808 (2021). doi:10.1002/qua.26808
- [63] K.P. Huber and G. Herzberg, *Molecular Spectra and Molecular Structure: IV. Constants of Diatomic Molecules* (Van Nostrand, New York, USA, 1979).
- [64] U.M. Ascher and L.R. Petzold, *Computer Methods for Ordinary Differential Equations and Differential-Algebraic Equations* (Society for Industrial and Applied Mathematics, Philadelphia, PA, USA, 2009).
- [65] E. Hairer, S.P. Nørsett and G. Wanner, *Solving Ordinary Differential Equations I: Nonstiff Problems* (Springer-Verlag, Berlin, Heidelberg, 1993).
- [66] C.R. Harris, K.J. Millman, S.J. van der Walt, R. Gommers, P. Virtanen, D. Cournapeau, E. Wieser, J. Taylor, S. Berg, N.J. Smith, R. Kern, M. Picus, S. Hoyer, M.H. van Kerkwijk, M. Brett, A. Haldane, J.F. del Rio, M. Wiebe, P. Peterson, P. Gérard-Marchant, K. Sheppard, T. Reddy, W. Weckesser, H. Abbasi, C. Gohlke and T.E. Oliphant, *Nature* **585**, 357–362 (2020). doi:10.1038/s41586-020-2649-2
- [67] T.E. Oliphant, *Guide to NumPy* (Trelgol Publishing, USA, 2006).
- [68] W.H. Press, S.A. Teukolsky, B.P. Flannery and W.T. Vetterling, *Numerical Recipes in Fortran (The Art of Scientific Computing)* (Cambridge University Press, New York, 1993), pp. 140–150.
- [69] T.N.L. Patterson, *Math. Comput.* **22**, 847–856 (1968). doi:10.1090/mcom/1968-22-104
- [70] T.N.L. Patterson, *Math. Comput.* **23**, 892 (1969). doi:10.1090/mcom/1969-23-108
- [71] R. Piessens, E. de Doncker-Kapenga, C. Überhuber and D. Kahaner, *Quadpack – A Subroutine Package for Automatic Integration* (Springer-Verlag, Berlin, Heidelberg, 1983).
- [72] A. Raj and Y.B. Chao, A repository containing a Python module and sets of functions for PES determination from expt. data on transition frequencies, computing polarizability matrix elements and Raman intensities, <https://github.com/ankit7540/Raman-Intensity-Approxmn-Test> (accessed December 23, 2021) (2022).
- [73] P. Schwerdtfeger and J.K. Nagle, *Mol. Phys.* **117**, 1200–1225 (2019). doi:10.1080/00268976.2018.1535143
- [74] G. Maroulis, *Chem. Phys. Lett.* **442**, 265–269 (2007). doi:10.1016/j.cplett.2007.06.024
- [75] A. Raj, H.A. Witek and H. Hamaguchi, *J. Raman Spectrosc.* **52**, 1032–1047 (2021). doi:10.1002/jrs.v52.5
- [76] D.A. Long, *The Raman Effect: A Unified Treatment of the Theory of Raman Scattering by Molecules* (John Wiley & Sons Ltd, Chichester, England, 2002).
- [77] A. Raj, H.A. Witek and H. Hamaguchi, *Asian J. Phys.* **30**, 321–335 (2021).
- [78] A. Raj, C. Kato, H.A. Witek and H. Hamaguchi, *J. Raman Spectrosc.* **51**, 2066–2082 (2020). doi:10.1002/jrs.v51.10
- [79] A. Raj, C. Kato, H.A. Witek and H. Hamaguchi, *J. Raman Spectrosc.* **52**, 2038–2050 (2021). doi:10.1002/jrs.v52.12
- [80] E. Jones, T.E. Oliphant and P. Peterson *et al.*, SciPy: Open source scientific tools for Python 2001, <https://www.scipy.org/> (accessed February 22, 2019).
- [81] P. Virtanen, R. Gommers and T.E. Oliphant *et al.*, *Nat. Methods* **17**, 261–272 (2020). doi:10.1038/s41592-019-0686-2